Technical Report

TR-09-08

Reduction of Pu(VI) on Fe surfaces: soft x-ray absorption and resonant inelastic scattering study

S M Butorin, K O Kvashnina, A Modin, J Nordgren,
Department of Physics and Materials Science, Uppsala University

J-H Guo, Advanced Light Source,
Lawrence Berkeley National Laboratory, Berkeley CA, USA

D K Shuh, Chemical Science Division,
Lawrence Berkeley National Laboratory, Berkeley CA, USA

L Werme, Svensk Kärnbränslehantering AB

March 2009

Svensk Kärnbränslehantering AB
Swedish Nuclear Fuel
and Waste Management Co

Box 250, SE-101 24 Stockholm
Phone +46 8 459 84 00

Reduction of Pu(VI) on Fe surfaces: soft x-ray absorption and resonant inelastic scattering study

S M Butorin, K O Kvashnina, A Modin, J Nordgren,
Department of Physics and Materials Science, Uppsala University

J-H Guo, Advanced Light Source,
Lawrence Berkeley National Laboratory, Berkeley CA, USA

D K Shuh, Chemical Science Division,
Lawrence Berkeley National Laboratory, Berkeley CA, USA

L Werme, Svensk Kärnbränslehantering AB

March 2009

Contents

1 Introduction

Many of the fission products and actinides that are produced during irradiation of uranium dioxide fuel in a light water reactor have several valence states. The properties of these elements in water solutions can be very different depending on the oxidation state. The general trend is that their solubilities increase with oxidation. Uranium, for example, has a solubility of about 10^{-9} mol/kg as U(IV) in carbonate containing mildly alkaline groundwaters, where $U(OH)_4$ is expected to be the dominant solution species. As U(VI), the corresponding solubility would be 5 orders of magnitude higher with uranyl carbonates as dominating solution species. Obviously, such differences in solubilities will have a large impact on the rate of release of radioactivity from a repository to the biosphere.

Deep groundwaters in granitic rock are found to be oxygen free and reducing. The more reduced forms of these elements are, therefore, expected to be the stable forms in these waters. Because of its radioactivity, however, the spent fuel will be capable of decompose the water by radiation. This radiolysis will produce equivalent amounts of oxidizing and reducing species and should, therefore, not affect the redox potential of the system. The main reducing species produced is hydrogen and hydrogen is known to be relatively inert at lower temperatures. The oxidizing species, on the other hand, are very reactive and this difference in reactivity of the oxidizing and reducing species is believed to create an oxidizing environment close to the fuel. As a consequence of that, radionuclides may dissolve from the fuel as more oxidized species and, therefore, in larger amounts. Once oxidized, a subsequent reduction when the dissolved species enter a reducing environment may be slow or even hindered. As an example, sulphate ions are stable, in the absence of bacteria, over geological time periods in solutions where sulphide is the thermodynamically stable form of sulphur.

There are a number of fission products and also other actinides that can occur in different oxidation states that have different solubilties in water. The most important one is plutonium, which has a very low solubility as Pu(IV), while Pu(V) and Pu(III) have much higher solubilities.

In prior studies, the Ultra-Soft X-ray Group at Uppsala University has shown that it is possible to determinate the oxidation state of uranium sorbed and reduced onto anaerobically corroding iron from a solution of uranyl carbonate using resonant inelastic soft x-ray scattering (RIXS). It has been also demonstrated that it is possible to monitor in situ the kinetics of this reduction process using a specially designed reaction cell. In present report, the possibilities to apply RIXS to study the reducibility and reduction kinetics of plutonium are described based on model calculations and experimental results obtained. As Pu only exist as radioactive isotopes, that aspect should also be considered when assessing the possibilities to study them experimentally in facilities that the Ultra-Soft X-ray Group at Uppsala University has access to.

2 Technique and models

To successfully describe various physical properties of a system in question it is necessary to obtain knowledge about the ground state and low-energy excited states of this system. For transition element, lanthanide, and actinide compounds with a partly filled *d* or *f* shell, strong correlation effects, when the dispersional part of *d* or *f* bandwidth is smaller than the on-site Coulomb interaction *U* between localized electrons, break down a single-particle picture and an atomic-like approach to characterize the electronic structure of these compounds is more appropriate.

In this case a state of the system without a core hole is described in terms of intra-atomic neutral excitations (a multiplet structure of the ground state electronic configuration due to electrostatic, exchange, crystal field, spin-orbit interactions, etc.) and/or inter-atomic charge-transfer excitations. The latter are the result of electron hopping from delocalized states to a localized state and are treated by short-range models, such as an Anderson impurity model /1/, using a set of parameters. The models are represented by the Hamiltonian

$$H = \sum_{k,\alpha,\sigma} \varepsilon_{k\alpha} n_{k\alpha\sigma} + \sum_{m,\sigma} \varepsilon_m n_{m\sigma} + \sum_{k,\alpha,m,\sigma} (V_{k\alpha m} \psi^{\dagger}_{m\sigma} \psi_{k\alpha\sigma} + H.c.) + U \sum_{m,m',\sigma,\sigma'} n_{m\sigma} n_{m'\sigma'} \qquad \text{(Eq. 2-1)}$$

Important physical quantities included in this Hamiltonian are the delocalized- and localized-state energies $\varepsilon_{k\alpha}$ and ε_m, hopping matrix element $V_{k\alpha m}$, and U. Here k, α, σ, and m denote a wave vector, an index of the energy level in the valence band, a spin index, and an azimutal quantum number, respectively. For the description of core spectroscopies a further term is added to the Hamiltonian to account for coupling between localized electron and a core hole. The values of model parameters are optimized by fitting both high-energy spectroscopic and low-energy transport data and then employed to describe the character of the ground state, different ground-state properties, the nature and size of the band gap in insulators /2/, etc.

Since the interpretation of transport measurements in these regards is often hampered by the presence of defects and by the importance of electron-lattice interactions, high-energy spectroscopies which directly probe the electronic degrees of freedom are often used for preliminary estimations of model parameters. In these estimations, it is important to take into account significant configurational dependence of model parameters which is predicted by first-principles calculations /3/. In particular, removing/adding of a valent *d* or *f* electron is expected to result in a decrease/increase in the value of the hybridization strength *V* which in turn may lead to renormalization effects for *U*. These effects are more pronounced for core-level spectroscopies. In the presence of a core hole *V* is strongly reduced since the waverfunctions become more localized. The renormalization of model parameters in the final state can produce a significant uncertainty in estimated values of these parameters in the ground state. In this situation, x-ray scattering techniques become very attractive because the scattering process is charge-neutral.

By now, it has been proven that at some core-thresholds of electron-correlated systems x-ray emission spectroscopy with monochromatic photon excitation can be considered as an analog of these techniques so that the excitation-radiative deexcitation channel can be treated as resonant inelastic x-ray scattering (RIXS) process. Final states probed via such a channel are related to eigenvalues of the ground state Hamiltonian. The core-hole lifetime is not a limit on the resolution in this spectroscopy (see e. g. /4/). It is important to distinguish between the many-body description of RIXS and a single-particle approach which is usually applied to wide-band materials /5/. The differences between two formalisms are schematically illustrated in Figure 2-1.

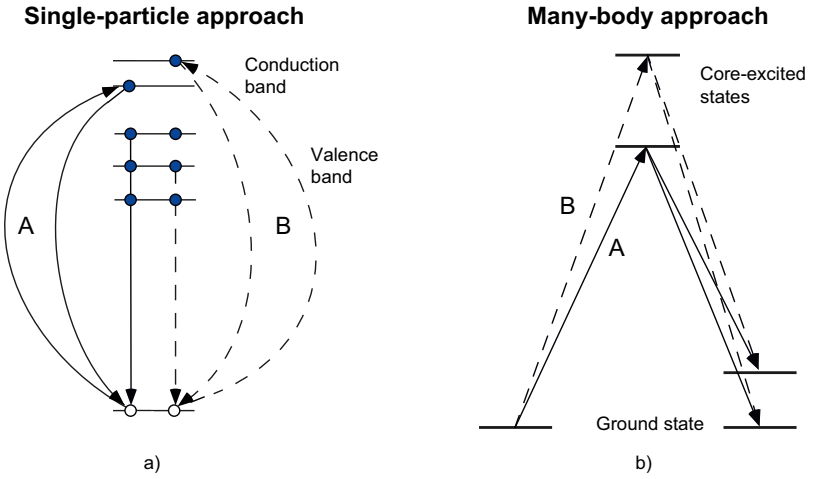

Figure 2-1. *Schematic representation of the radiative deexcitation process for two different core excitations A and B.*

According to the many-body picture, an energy of a photon, scattered on a certain low-energy excitation, should change by the same amount as a change in an excitation energy of the primary beam (see a decay route of core excitation *B* versus that of *A*) so that inelastic scattering structures have constant energy losses and follow the elastic peak on the emitted-photon energy scale. In the single-particle view, energy positions of specific inelastic-scattering structures with respect to the elastic peak which are defined by the momentum conservation rule may vary only within the energy range covered by the occupied part of the valence band. In Figure 2-1a, this is reflected in the situation when, for core excitation *B* with the higher energy, the radiative decay results in a transition with the lower energy than those for *A*, respectively. In spite of simplifications made here, the outlined differences can be used to test the validity of one or another model for a system in question.

As an example, we use data from /6/ (see Figure 2-2) which were obtained at the U $3d_{5/2}$ edge of UO_3. The inelastic scattering structure with the energy loss of about 5 eV is observed to follow the elastic peak up to 20 eV above the $3d_{5/2}$ threshold while the width of the occupied part of the valence band is only ~4 eV. This indicates the importance of electron correlation effects in UO_3. Similar results were obtained at the U 5*d* edge of this oxide (Figure 2-3).

Although, the information provided by the RIXS technique is similar to that obtained from optical absorption or low-energy electron-energy-loss (EELS) spectroscopies, there are some advantages in using this method:

1. the technique is not surface-sensitive, helping to avoid the confusion with a formation of additional states because of surface defects;
2. its element-specificity enables one to study of even very dilute compounds since metal states can be probed separately from ligand states;
3. the cross-section for inelastic x-ray scattering is strongly enhanced on the resonance in contrast to weak dipole-forbidden transitions in optical absorption spectra;
4. the dipole nature of radiative transitions makes it easier to calculate RIXS intensities compared to *d-d* (*f-f*) intensities in optical spectroscopy or in EELS.

In calculations of resonant x-ray scattering as a second order optical process, only a resonant term of the modified Kramers-Heisenberg equation is usually used, where the spectral intensity is given by

$$I_{qq'}(\Omega,\omega) = \sum_f \left| \sum_i \frac{\langle f | T_{q'} | i \rangle \langle i | T_q | g \rangle}{E_g + \Omega - E_i - i\Gamma_i/2} \right|^2 \delta(E_g + \Omega - E_f - \omega).$$

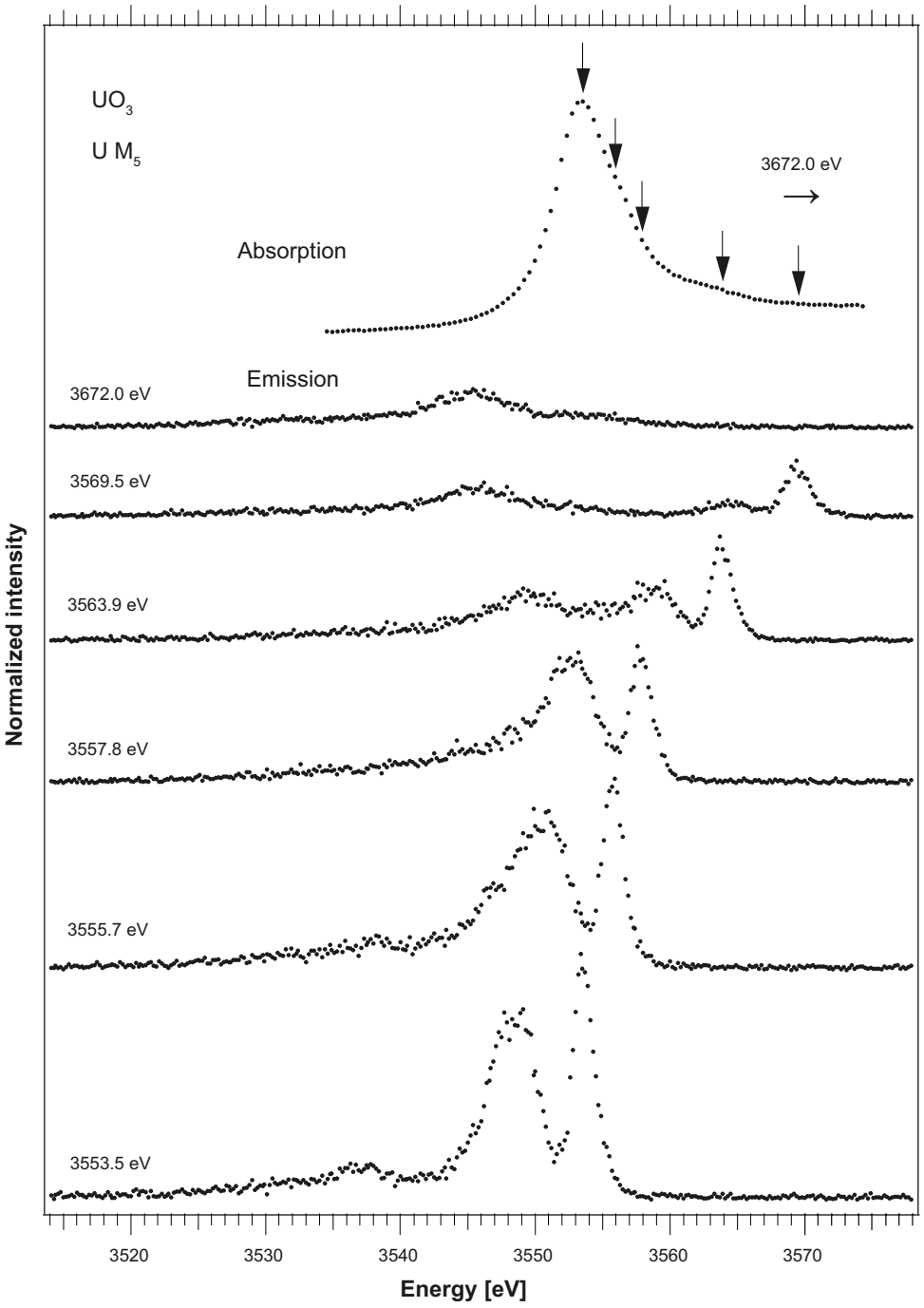

Figure 2-2. *U M5 x-ray photon-in-photon-out spectra recorded across the U $3d_{5/2}$ threshold of UO_3 /6/. Excitation energies used in these measurements are indicated by arrows on the absorption spectrum.*

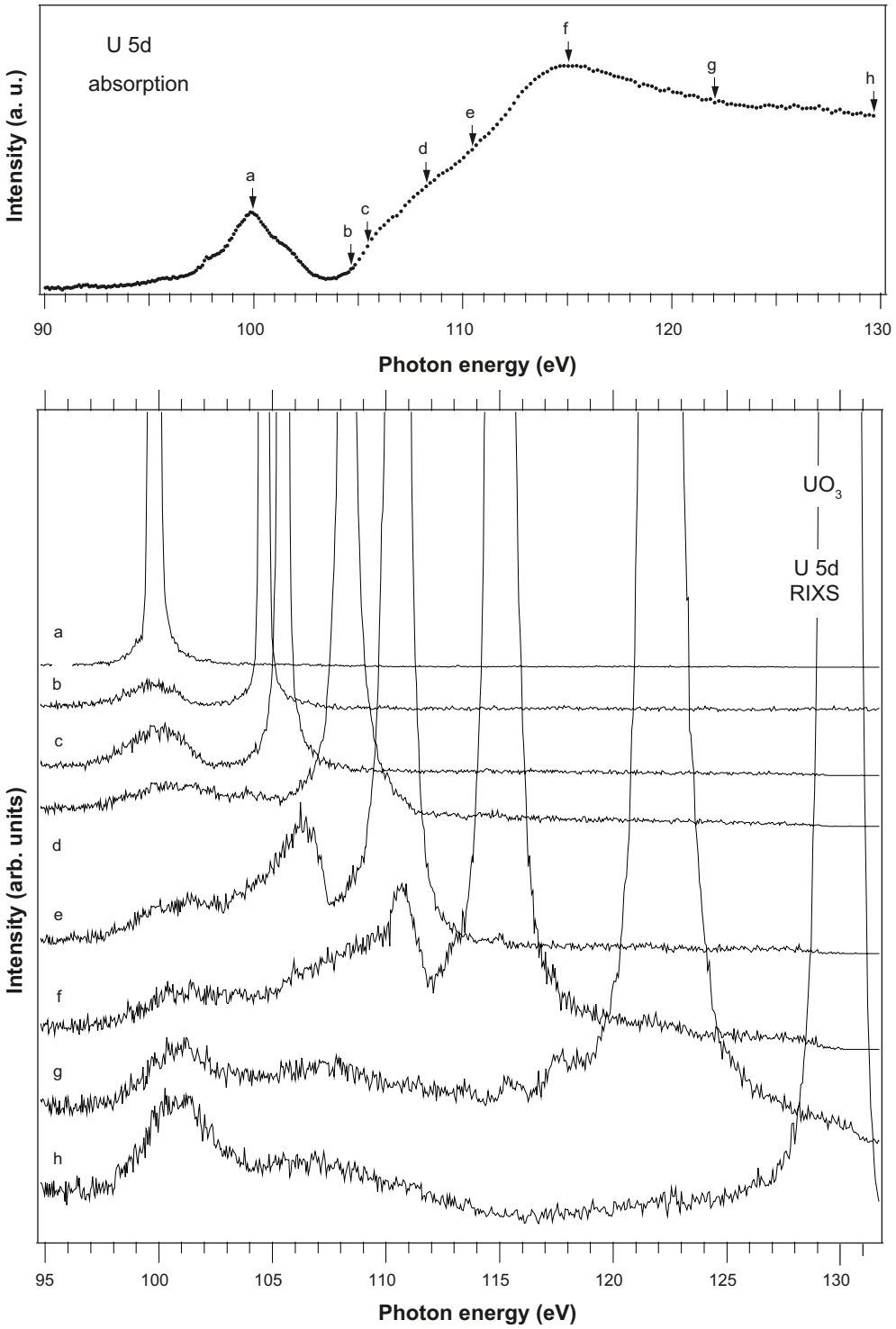

Figure 2-3. *Resonant inelastic x-ray scattering spectra recorded across the U 5d edge of UO_3. Excitation energies used in these measurements are indicated by arrows on the absorption spectrum.*

Here, $|g\rangle$, $|i\rangle$, and $|f\rangle$ are the ground, intermediate, and final states with energies E_g, E_i, and E_f, respectively, while Ω and ω represent energies of incident and scattered photons, respectively. D is the dipole operator, Γ stands for the intermediate state lifetime and q and q' are polarizations of the light with respect to the quantization axis.

For the case of studying the multiplet structure of the ground state configuration, the ability of resonant photon-in-photon-out spectroscopy to probe low-energy excitations was first discussed by Tanaka and Kotani /8/ in the description of resonant spectra of La_2CuO_4 and CuO at the Cu 2*p* edge. The difference in *d*-*d* excitation profiles for $3d^9$ multiplets between these two oxides was predicted. However, no experimental data were available with the energy resolution being sufficient enough to support conclusions made by authors. The first experiment which unambiguously confirmed the ability of this resonant technique to probe elementary excitations was performed /9/ on MnO (two years later, high-resolution RIXS data at the Cu 3*p* resonance of cuprates were published /4/ which are in good agreement with theoretical predictions). Prior to this, probing of *f*-*f* excitations in rare-earths was discussed in /10/. Figure 2-4 illustrates how RIXS structures due to *f*-*f* excitations in UF_4 resonantly enhanced for a number of energies of incident photons tuned to the U 5*d* threshold and how this structures (observed within 4 eV below the elastic peak) follow an elastic peak when sweeping the incident photon energies throughout the U 5*d* x-ray absorption edge.

The efficiency of the RIXS technique in studies of charge-transfer excitations for valence electrons in correlated systems was first demonstrated by Butorin et al. /6/ for both soft and intermediate-energy x-ray regions. Various aspects of probing the charge-transfer excitations by this spectroscopy and data interpretation within the Anderson impurity model framework are discussed extensively in the review by Kotani /11/. A reader is also referred to publications by present authors et al. /6, 12–14/ where the latter issue is addressed.

To better explain how the RIXS spectroscopic tool can be utilized for addressing the issue of Pu reducibility, examples of similar studies for uranium and neptunium are shown below.

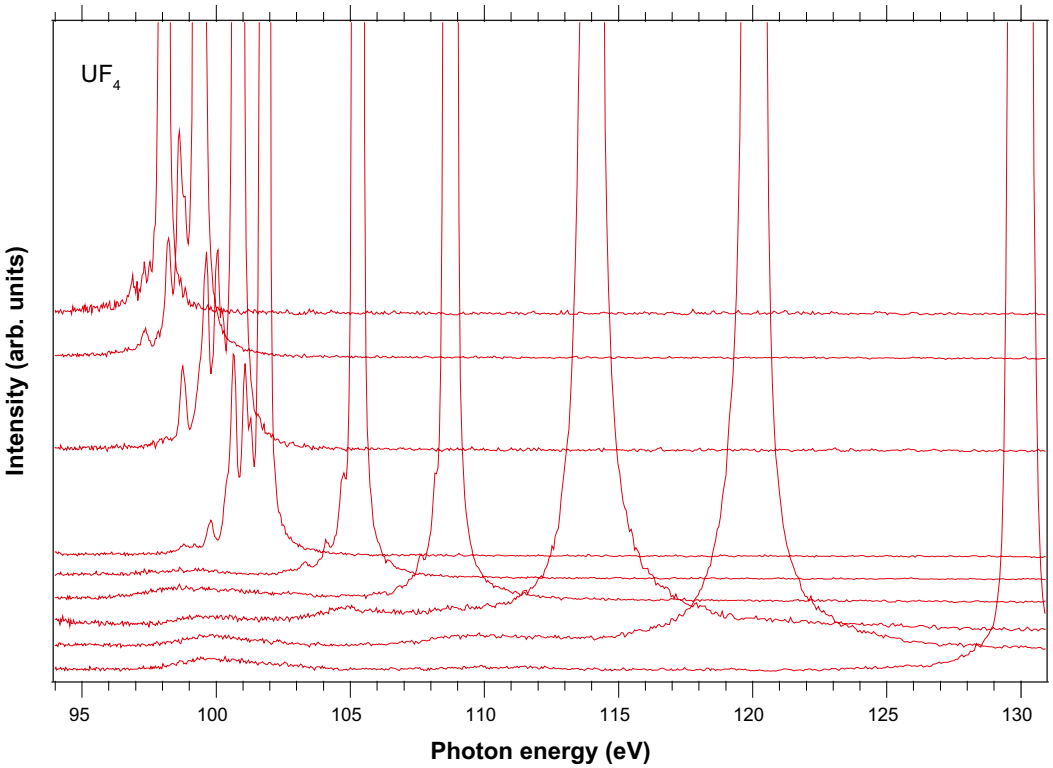

Figure 2-4. *Resonant inelastic x-ray scattering spectra recorded across the U 5d edge of UF_4 Strong elastic peaks indicate/correspond to energies of incident photon beam used to measure RIXS spectra.*

3 Uranium

The case of uranium is maybe the most illustrative for what RIXS technique can do. RIXS measurements at the U 5*d* threshold provide an opportunity to study in detail elementary excitations in U compounds due to the higher resolution of such experiments in comparison with those at the U 3*d* and 4*d* thresholds. It has turned out that the technique is very sensitive to the valency and the chemical state of uranium in contrast to x-ray absorption spectroscopy (XAS). Figure 3-1 shows x-ray absorption spectra of a number of U compounds recorded across the U 5*d* edge in the total electron yield mode. The 5*d* core-hole lifetime broadening is quite large, thus reducing the utility of XAS. As a result, the U 5*d* absorption spectra in Figure 3-1 do not exhibit sharp features. The substantial smearing of spectral structures hampers the analysis of the chemical state and the chemical environment of uranium in various compounds. In particular, it is difficult to distinguish between uranium species with different oxidation states, especially in case when one of species has a much lower concentration than another.

In this situation, the virtually unlimited resolution (defined by the response function of the instrument) of the RIXS technique and its ability to enhance transitions to specific excited states are especially useful. The RIXS profile strongly depend on the choice of the excitation energy. The spectral weight corresponding to electronic transitions within the 5f shell is enhanced at excitation energies close to 100 eV while at higher energies of the incident photon beam, set to

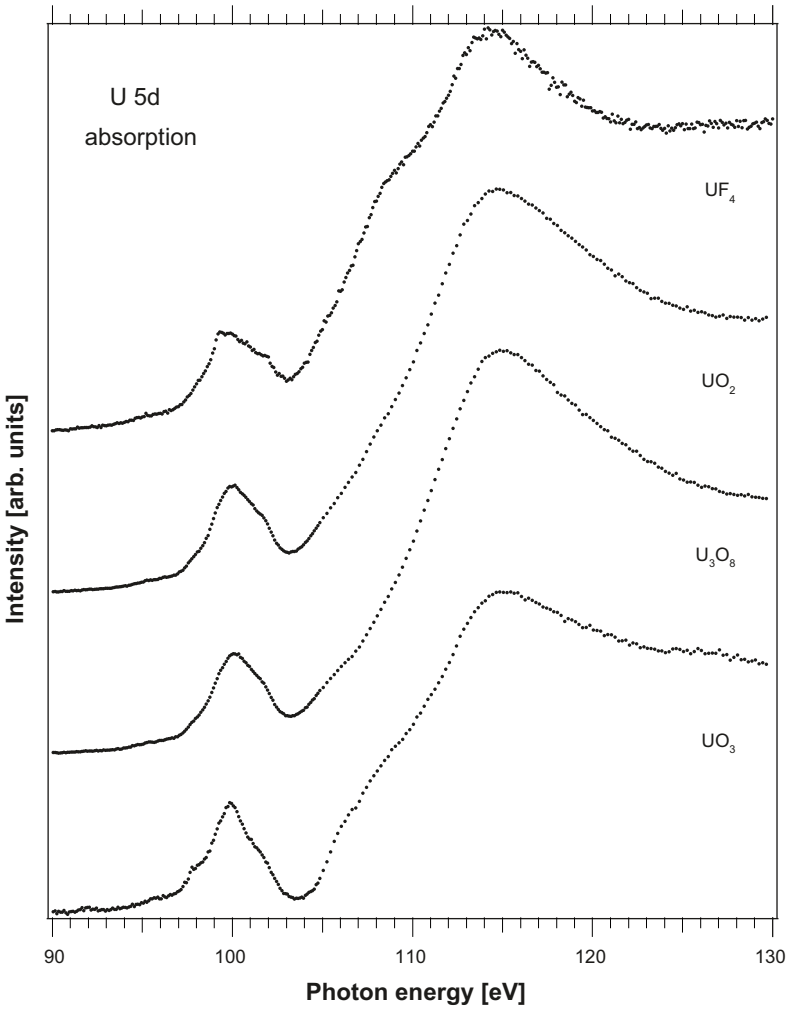

Figure 3-1. *Total electron yield spectra of UF_4, UO_2, U_3O_8, and UO_3 near the U 5d absorption edges.*

the main 5d absorption edge, inter-ionic excitations of charge-transfer character, such as ligand $2p \rightarrow$U $5f$ charge-transfer, dominate the RIXS spectra. This has been established by measurements on a set of model U compounds and by model calculations. The spectral pattern of intra-ionic *f-f* excitations is mainly determined by the formal valency of U, in turn, the charge-transfer transitions strongly depend on the chemical environment of U ions.

An example of probing the *f-f* excitations in U oxide is shown in Figure 3-2 where the RIXS spectra of solid UO_2, recorded for various incident photon energies in the pre-5*d*-threshold region, are displayed. The assignment of sharp inelastic scattering structures to the *f-f* transitions is supported by atomic multiplet calculations for the U^{4+} ion. The spectra were calculated using Equation 2-2. Matrix elements were obtained from Cowan's programs /15/ so that Slater integrals $F^k(5f, 5f)$, $F^k(5d, 5f)$, $G^k(5d, 5f)$, and $R^k(5d\varepsilon g, 5f)$ were scaled down to 75%, 75%, 66%, and 80%, respectively, from the Hartree-Fock values. The reduction factors for Slater integrals represent the effect of the intra-atomic configuration interaction, the same factors were used in a number of publications to successfully reproduce 4*d* XA and 4*d* photoemission spectra of

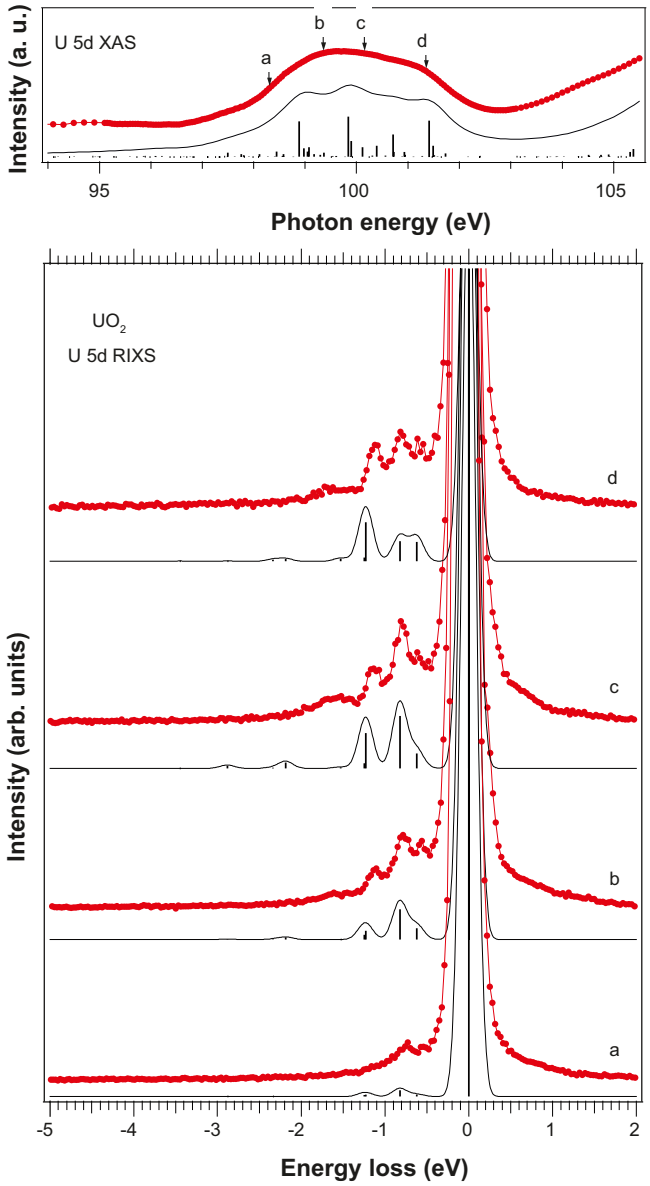

Figure 3-2. *Resonant x-ray scattering spectra of* UO_2 *recorded at different excitation energies close to the U 5d threshold (lines with markers) together with the results of atomic multiplet calculations (sticks with thin lines) for the U(IV) ion. Excitation energies are indicated by arrows on the total electron yield spectrum at the U 5d absorption edge shown in the top panel.*

various rare-earth systems /16–18/. The density of states of the continuum was assumed to be constant and the kinetic energy of the continuum electron was set to the value which made the average energies of $5d^9 5f^3$ and $5d^{10} 5f^1 \varepsilon g$ equal.

The calculations reproduce all of the spectral structures very well especially an enhancement of the peak at about 1.2 eV with increasing excitation energies. The growth of the peak is due to enhanced transitions into the $^1G_4$ state. Changes in absolute intensities of inelastic scattering structures corresponding to the *f-f* transitions are reproduced on going from spectrum *a* to spectrum *b*. For spectra *c* and *d*, such changes in calculated intensities are about three times higher as compared to those in the experiment. The discrepancy may originate from the normalization procedure for the experimental spectra to account for variations in the incident photon flux. The intensity of the elastic peak was used as a reference in this procedure. However, the elastic peak contains some contribution of diffuse scattering which may vary with varying excitation energies.

RIXS profiles, corresponding to the *f-f* excitations, are found to be very sensitive to the chemical state of U in different systems /19/. For example, it is a matter of the presence or absence of these excitations when going from U^{4+} to U^{6+} compounds. Therefore, RIXS measurements near the U 5*d* threshold provide good fingerprints for the chemical state of U in different systems in contrast to x-ray absorption spectra which show only small differences at the U 5*d* edge.

An example to show are our findings about the chemical state of U in U_3O_8 and reduced UO_3. In particular, for U_3O_8, it was discussed in literature that the chemical state of U is described as either $U^{VI}U_2^{V}O_8$ or $U_2^{VI}U^{IV}O_8$. To our knowledge, there is no clear and convincing answer to this question and it is still under debate. Thus, core-level photoemission /20–22/ and electron spin resonance /23, 24/ data have been interpreted in favor of either situation by different groups and therefore these techniques can not really provide unambiguous answer. It turns out that the RIXS technique can. RIXS spectra of *f-f* excitations are a good indicator of whether uranium is in the U(IV), U(V) or U(VI) state. The data are easy to interpret and not very difficult to calculate. Establishing the real chemical state of U in oxides is important for both applied, environmental and fundamental science (e.g. a development of theory of non-stoichiometry is a fundamental problem).

Figure 3-3 displays RIXS spectra of *f-f* transitions for a number of U oxides. Close similarity of the *f-f* transitions profile in U_3O_8 to those in UO_2 and UF_4 as well as to that calculated for the U(IV) ion (see Figure 3-2) unambiguously indicates the presence of the U(IV) fraction in U_3O_8, thus favoring the $U_2^{VI}U^{IV}O_8$ description of the uranium chemical state in this oxide. Furthermore, similar pattern is observed for reduced UO_3, thus indicating that oxygen deficiency leads to the creation of U(IV) species in the compound.

Charge-transfer effects are expected to be significant in actinide compounds as a result of metal 5*f*–ligand 2*p* hybridization. The analysis of our data /19/ obtained at U $3d_{5/2}$ threshold shows that the ligand 2*p* →U 5*f* charge-transfer plays an important role in uranium compounds, such as UO_2, $UO_2(NO_3)_2 \cdot 6H_2O$, and even in UF_4.

This is also supported by theoretical studies. Molecular-orbital calculations by several research groups /25–28/ gave values for the 5*f* occupancy, which range from 2.3 to 2.9 electrons, while this occupancy was estimated at about 2.3 electrons from the analysis of x-ray absorption and photoemission data within an Anderson impurity model /29, 30/. These results indicate significant degree of covalency for U–O chemical bonds in UO_2. For UF_4, a 5*f* contribution of ~0.3 electrons to the bonding orbitals was also predicted from relativistic Dirac-Slater local-density calculations /31/. For compounds containing U^{6+}, the degree of co-valency for metal–ligand bonds is expected to be even higher than that for U^{4+} systems. For example, molecular-orbital calculations yielded the 5*f* occupancy of ~2.6 electrons for the uranyl ion UO_2^{2+} /32, 33/. Although, the values for the 5*f* occupancy obtained from molecular-orbital calculations seem to be overestimated /34/ one can not rule out the importance of the U 5*f*-ligand 2*p* hybridization even in a compound with “ionic” bonds such as UF_4.

The consequences of high covalency and hybridization in the ground state is an appearance of charge-transfer satellites in high-energy spectroscopic data. Figure 3-4 illustrates the dependence of the RIXS spectra on the chemical environment of U atoms in various compounds. The spectra were measured under condition when the inelastic RIXS cross-section is enhanced for

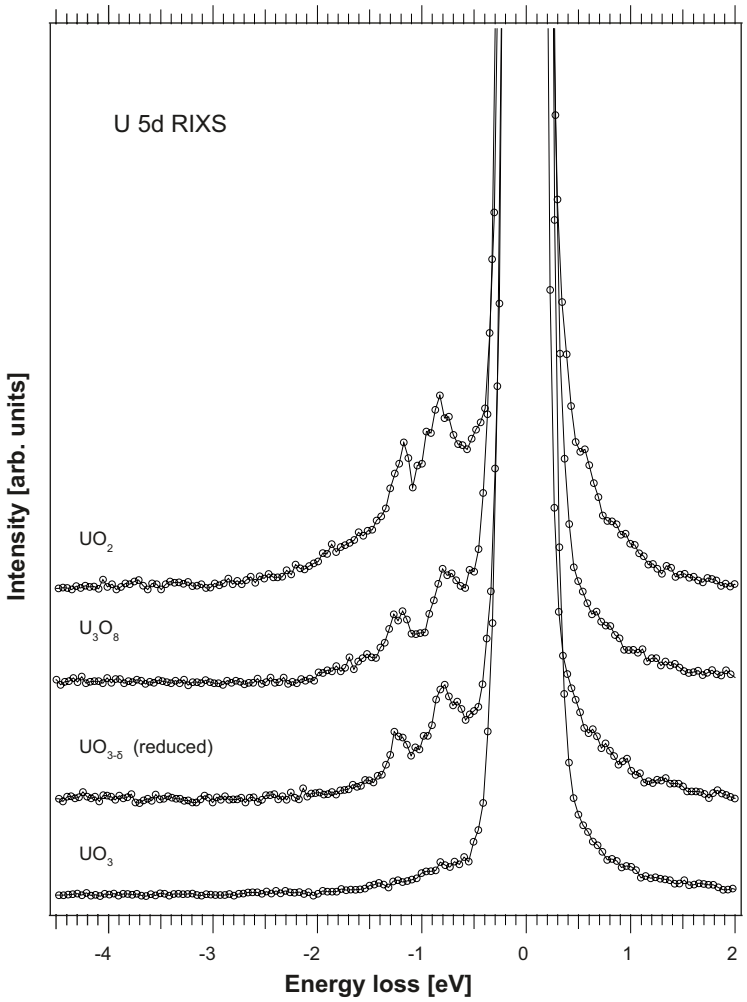

Figure 3-3. *Resonant inelastic x-ray scattering spectra of U oxides recorded at the incident photon energy of 99.9 eV.*

the ligand $2p \rightarrow$U $5f$ charge-transfer transitions, in particular, when the energy of the incident photon beam is tuned to the main edge of the U $5d$ x-ray absorption spectrum (see Figure 3-1). At these energies, the charge-transfer excitations dominate RIXS spectra, thus defining the RIXS profile. The profiles can be clearly divided into three groups: (i) UF_4, (ii) UO_3 and $UO_{3-\delta}$, (iii) U_3O_8 and UO_2. The differences between profiles determined by the character of the bonding and the local geometrical arrangement of ligands, i.e. local crystal structure.

In prior studies the Ultra-Soft X-ray Group at Uppsala University carried out spectroscopic analysis of various samples relevant for the processes of dissolution of uranium dioxide in groundwaters. The purpose of the work was to determine whether U(VI) can be reduced to U(IV) under conditions relevant to spent fuel disposal, in particular, reduction of U(VI) to U(IV) in the presence of actively corroding canister materials.

Measurements employing RIXS technique for a set of model samples were carried out at beamline 7.0 of the Advanced Light Source, Berkeley, USA. The material studied was a Fe foil polished with diamond spray (1 and 1/4 mm) on one side. The foil was exposed to solution containing U(VI) ions for 17 days. An aliquot of U(VI) was added in the form of uranyl nitrate solution to deaerated Allard groundwater (100 ml) under N_2 atmosphere. The starting concentration of U in solution was 500 ppb. RIXS measurements were performed in an attempt to establish whether the sorption of U(VI) ions onto the Fe surface resulted in some reduction of these ions to U(IV). The spectroscopy provides good signatures in terms of new distinct transitions, representing electronic excitations within the 5f shell and having a characteristic profile for U(IV).

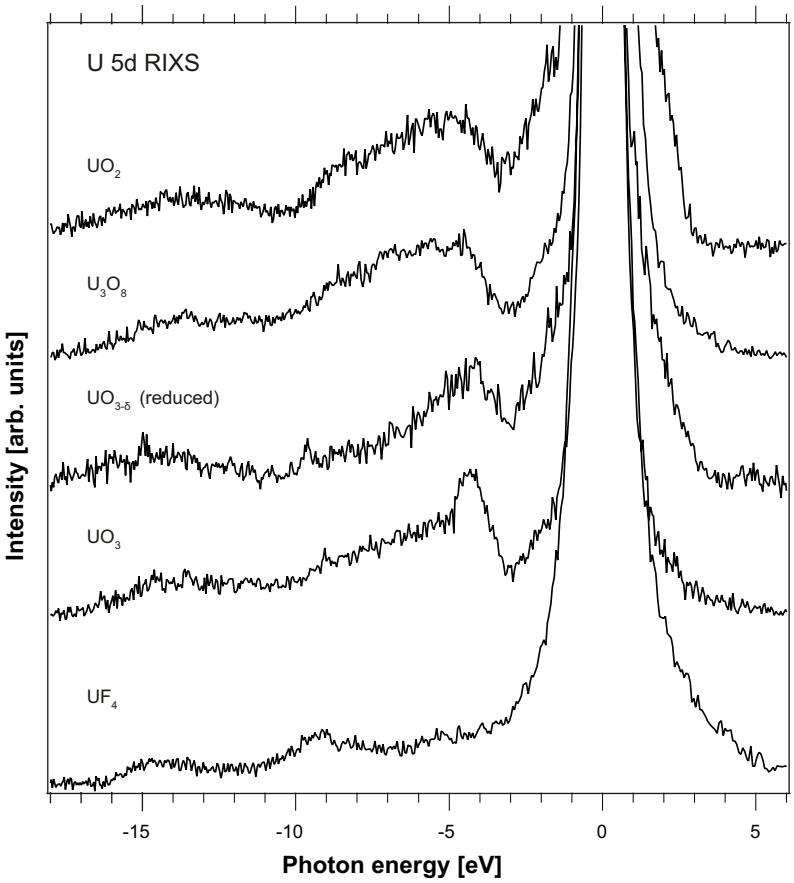

Figure 3-4. *Resonant inelastic x-ray scattering spectra of a number of U compounds recorded at the incident photon energy of 115.0 eV.*

Figure 3-5 displays a set of x-ray scattering data from the Fe sample recorded at the incident photon energy of 100 eV which corresponds to the energy of the weak pre-threshold structure in the U 5*d* x-ray absorption spectrum. A series of spectra were randomly measured from different 1mm x 150mm areas on the Fe sample surface. Six of them are shown in the figure along with spectra of reference oxides UO_2 and UO_3 that contain U(IV) and U(VI), respectively. Setting the energy of the incident beam close to the U 5*d* thresholds enhances the inelastic scattering cross-section and ensures that electronic states of 5*f* symmetry are probed by the spectroscopy due to dipole selection rules. The choice of the excitation energy is also defined by the necessity to selectively look at the intra-ionic *f-f* transitions of U. The spectral weight corresponding to these transitions is enhanced at an excitation energies close to 100 eV.

An inspection of Figure 3-5 shows the presence of two distinct RIXS structures at energy losses of about –0.8 and –1.15 eV in the UO_2 spectrum. These structures represent *f-f* transitions as incident x-rays are inelastically scattered on electronic excitations within 5*f* shell. The structures are very well reproduced by model calculations of RIXS spectra using atomic multiplet theory for the U(IV) ion. Naturally, these structures are absent in the UO_3 spectrum due to the formal $5f^0$ configuration of the U(VI) ions. In this situation, any reduction of U(VI) on the Fe surface should result in an appearance of characteristic RIXS structures. The present measurements indeed reveal the presence of significant inelastic weight in spectra recorded from some areas (spectra 4–6) on the surface of the Fe sample, thus indicating U(VI) reduction in those areas.

However, a comparison of RIXS spectra of the charge-transfer transitions between the foil and UO_2, made in Figure 3-6, suggests that U(IV) species on the Fe foil are not necessarily in the form of uranium dioxide. The RIXS profiles of compared spectra are somewhat different.

Similar results were obtained for another Fe foil prepared under the same conditions but with much longer exposure (8.5 month) to the U(VI) solution.

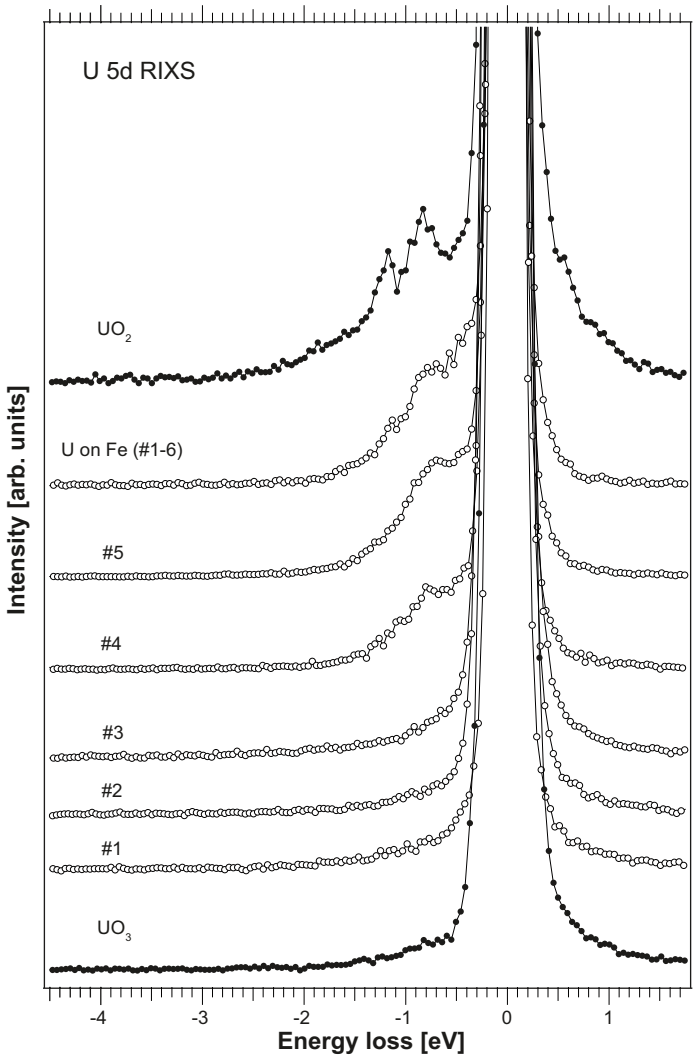

Figure 3-5. *Enhanced inelastic part of the soft x-ray scattering spectra of UO_2 and UO_3 and UO_2^{2+} adsorbed on the Fe foil (elastic peaks are at 0 eV). The energy of the incident photons was set to 100 eV. The incidence angle of the photon beam to the sample surface was about 15°. Scattered x-rays were detected at the right angle to the direction of the incident beam in the horizontal scattering plane. The six spectra of adsorbed U were randomly measured from different 1mm x 150mm areas on the surface of the Fe sample.*

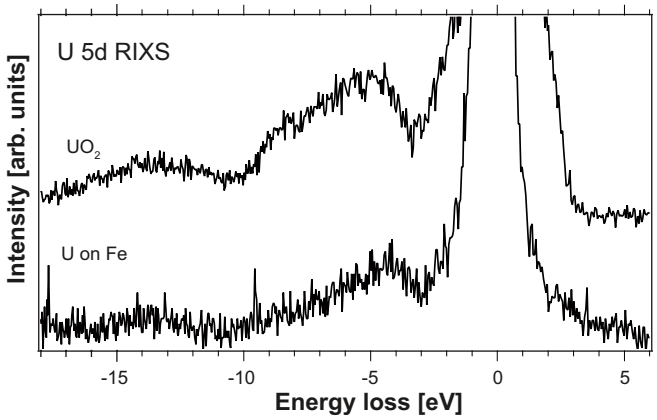

Figure 3-6. *Enhanced inelastic part of the soft x-ray scattering spectra of UO_2 and UO_2^{2+} adsorbed on the Fe foil recorded at the excitation energy of 115.0 eV.*

4 Neptunium

The same kind of RIXS measurements were also made for the Np-on-Fe sample prepared at the Chalmers University in similar manner as above discussed Fe samples with sorbed UO_2^{2+}. Figure 4-1 shows a number of RIXS spectra of NpO_2 used as a reference system with the defined oxidation state for Np. The spectra were recorded at energies of the incident photon beam set to the pre-threshold structure in the Np 5*d* x-ray absorption spectrum. At such energies, the x-ray scattering cross-section is enhanced for *f-f* transitions. The energy losses of corresponding RIXS structures observed in Figure 4-1 are in agreement with optical absorption measurements of *f-f* transitions in Np(IV) systems /35, 36/.

The spectra in Figure 4-1 are compared with the results atomic multiplet calculations for the Np(IV) ion. The calculations were performed in similar manner as described for the case of U(IV) in the previous section, only this time the $F^k(5f, 5f)$ integrals were scaled down to 70%. The initial and final states of scattering process were taken to be those of the $5f^3$ configuration with the intermediate states of $5d^9 5f^4$ character which are mainly autoionized to $5f^2 \varepsilon g$ states. The calculated spectra show slight differences in the energy position for some RIXS structures when compared with experimental spectra. This is likely due to the influence of the crystal field interaction and/or the Np 5*f*-O 2*p* hybridization which were not taken into account in the calculations. The extra-structure observed in experimental spectra at an energy loss of around 950 meV may also be a result of the crystal field interaction. Nevertheless, the present calculations account for the overall RIXS profile and behavior and reproduce its dependence on the excitation energy.

Figure 5-1 displays RIXS spectra of Np sorbed on the Fe strip along with NpO_2 spectra recorded at the same excitation energies. An inspection of this figure shows that the RIXS structures of both samples closely resemble each other. This resemblance unambiguously indicates the existence of Np in the form of Np(IV) on the studied Fe stripe.

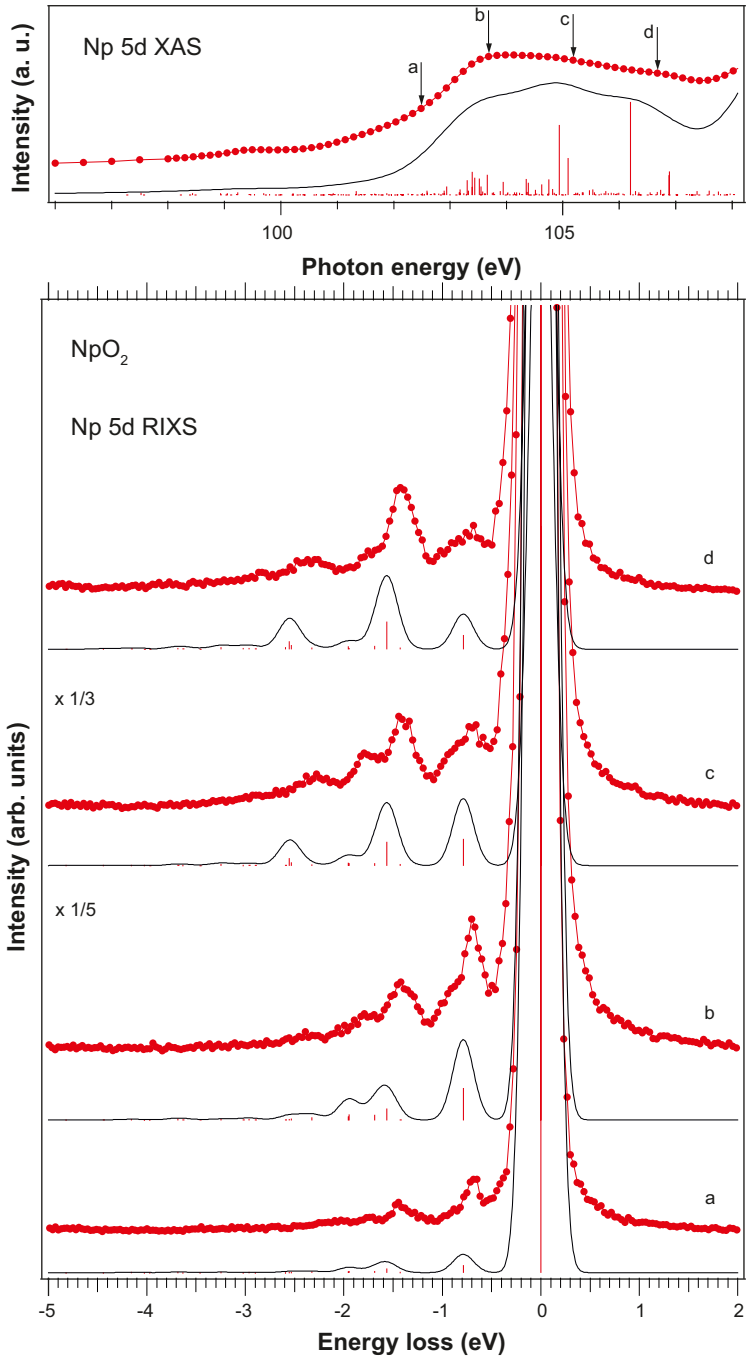

Figure 4-1. *Resonant x-ray scattering spectra of NpO_2 recorded at different excitation energies close to the Np 5d threshold (lines with markers) together with the results of atomic multiplet calculations (sticks with thin lines) for the Np^{4+} ion. Excitation energies are indicated by arrows on the total electron yield spectrum at the Np 5d absorption edge shown in the top panel.*

5 Plutonium

The examples described above show that the RIXS technique is quite efficient and successful in studies of the reducibility and reduction kinetics of highly oxidized fission product and light actinide species. In this section, we examine the capabilities of RIXS spectroscopy when applied to plutonium systems.

5.1 Model calculations

As shown for U and Np compounds, the atomic multiplet theory is a good first approximation to interpret experimental data and describe RIXS spectral profiles and their changes. In order to understand how efficient the RIXS technique can be in this particular case, we performed model calculations for Pu(III), Pu(IV) and Pu(V) systems. Both x-ray absorption and resonant soft x-ray scattering spectra were calculated for the Pu 5*d* edges.

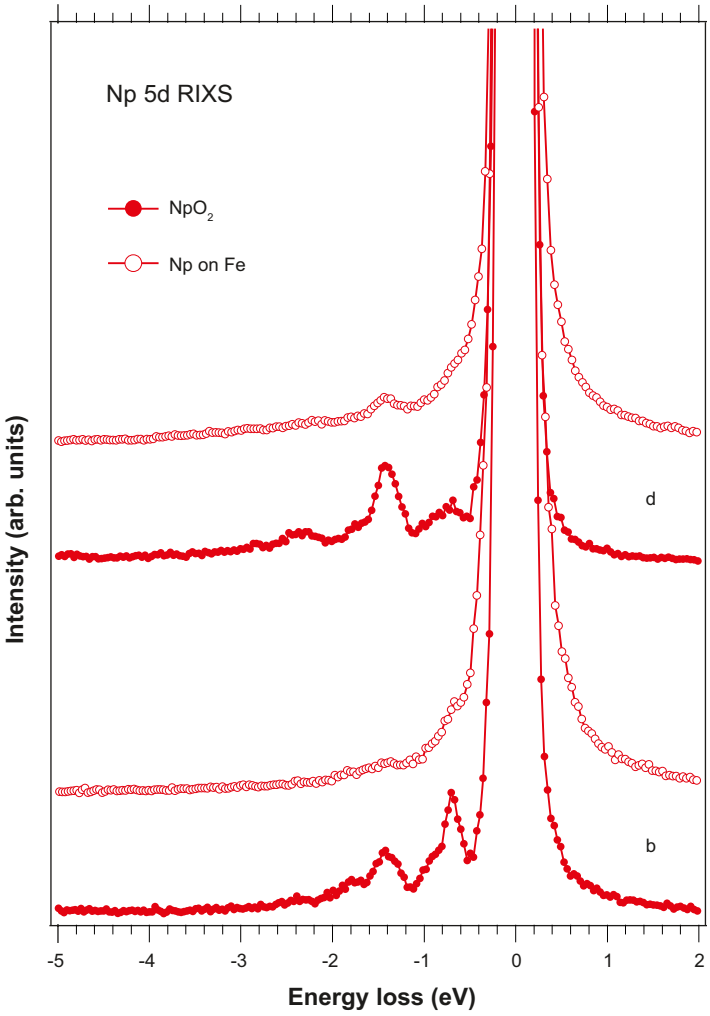

Figure 5-1. *Comparison of resonant inelastic soft x-ray scattering spectra of Np sorbed on the Fe strip and NpO_2. Letters correspond to the same excitation energies as in Figure 4-1.*

The x-ray absorption calculations were performed in similar fashion as described in /37/. Besides the $5d \rightarrow 5f$ excitation process these calculations included the $5d$-$5f5f$ super-Coster- Kronig decay from the excited state and the interference effect (Fano effect) with the direct $5f \rightarrow \varepsilon l$ excitation process.

The Hamiltonian of the system can be written as

$$H = H_0 + V_r + V_a, \qquad \text{(Eq. 5-1)}$$

where H_0 describes the Coulomb, exchange and spin-orbit interactions, V_r represents the radiative dipole $5d \rightarrow 5f$ and $5f \rightarrow \varepsilon l$ transitions, and V_a is super-Coster-Kronig transition of the $\langle 5d^9 5f^{n+1} | 1/r | 5d^{10} 5f^{n-1} \rangle$ type. H_0 works in a single configuration while V_r and V_a connect two different configurations. The symmetry of the continuum l is limited to g which provides the dominant path and the largest matrix elements. The $5d \rightarrow 5f$ excitation spectra are obtained by calculating the total yield of the resonant $5d \rightarrow 5f$ photoemission process. The XAS spectrum can be expressed as

$$I(\omega) = \int d\epsilon F(\epsilon, \omega). \qquad \text{(Eq. 5-2)}$$

Here $F(\varepsilon,\omega)$ represent the resonant photoemission spectrum

$$F(\epsilon, \omega) = \sum |\langle k\beta | T | g \rangle|^2 \delta(\hbar\omega + E_g - E_{k\beta}) \delta(\varepsilon - \varepsilon_k), \qquad \text{(Eq. 5-3)}$$

where $\hbar\omega$ is the incident photon energy, ε is the kinetic energy of the photoelectron, $|g\rangle$ stands for the ground state of H_0 in the $5f^n$ configuration, $|k\beta\rangle$ corresponds to the final states of $5f^{n-1}\varepsilon l$ configuration, E_g and $E_{k\beta}$ are the ground state and final state energies, respectively. The interaction between the continuum electron and the system left behind was ignored in calculations, so that the final states $|k\beta\rangle$ and their energies $E_{k\beta}$ can be decoupled as $|k\beta\rangle = |k\rangle|\beta\rangle$ and $E_{k\beta} = E_k + E_\beta$. Here $|k\rangle$ and E_k represent the εl continuum electron state and its energy and $|\beta\rangle$and E_β are the states of the f^{n-1} configuration and their energies, respectively.

The T operator is the t-matrix

$$T = V_r + V_a \frac{1}{z - H_0} T \qquad \text{(Eq. 5-4)}$$

with

$$z = \hbar\omega + E_g + \imath\eta, \quad (\eta \rightarrow +0), \qquad \text{(Eq. 5-5)}$$

which is first order in the dipole operator V_r and infinite order in the Coulomb decay operator V_a.

From Equations 5-3 and 5-4, a new expression can be derived from some algebra

$$\begin{aligned} F(\epsilon, \omega) = & \sum_{k\beta} \langle k\beta | V_r | g \rangle + \sum_{\alpha,\alpha'} \langle k\beta | V_a | \alpha \rangle \langle \alpha | G | \alpha' \rangle \\ & \times \left(\langle \alpha' | V_r | g \rangle + \sum_{k'\beta'} \frac{\langle \alpha' | V_a | k'\beta' \rangle \langle k'\beta' | V_r | g \rangle}{z - E_{k'\beta'}} \right)^2 \\ & \times \delta(\hbar\omega + E_g - E_{k\beta}) \delta(\varepsilon - \varepsilon_k), \end{aligned} \qquad \text{(Eq. 5-6)}$$

where $|\alpha\rangle$ represents the excited states of the $5d^9 5f^{n+1}$ configuration and E_α is their energy. The Green function $\langle\alpha|G\rangle|\alpha'\rangle$ was obtained numerically by matrix inversion from

$$\langle \alpha | G | \alpha' \rangle = \frac{1}{z - E_\alpha} \delta_{\alpha\alpha'} + \frac{1}{z - E_\alpha} \sum_{k\beta,\alpha''} \frac{\langle \alpha | V_a | k\beta \rangle \langle k\beta | V_a | \alpha'' \rangle}{z - E_{k\beta}} \langle \alpha'' | G | \alpha' \rangle. \qquad \text{(Eq. 5-7)}$$

The reduced matrix elements required for present calculations were obtained with Cowan's programs /15/. The Slater integrals F^k, G^k, R^k, spin-orbit constants ζ, and radial integrals $(nl|r|n'l')$ were calculated by the Hartree-Fock program with relativistic correction. The values of $F^k(5f, 5f)$, $F^k(5d, 5f)$, $G^k(5d, 5f)$, and $R^k(5d\varepsilon g, 5f^2)$ were reduced to 80%, 75%, 66%, and 80%, respectively. The other parameters were used without reduction. The density of states in the continuum were assumed to be constant so that the R^k and dipole integrals were constant over the whole excitation region. The kinetic energy of the continuum electron was chosen to make the total average energies of $5d^9 5f^{n+1}$ and $5d^{10} 5f^{n-1} \varepsilon g$ configurations identical.

The decay half-width of the core-excited states is expressed as

$$\Gamma_\alpha = \pi \left| \langle k\beta \,|\, V_a \,|\, \alpha \rangle \right|^2 \qquad \text{(Eq. 5-8)}$$

and was computed for all the states in present calculations. The other decay channels omitted in the calculations were approximated by including an additional Lorentzian with the width of 1 eV.

The results of calculations of Pu 5d x-ray absorption spectra for different chemical states of Pu are displayed in Figures 5-2 to 5-4 along with computed Γ_α values. Γ_α significantly varies across the 5*d* edge. It has small values for the structure below the ionization threshold but increases substantially above this threshold. The increase causes a large broadening of the states contributing to the main edge so that the significant difference between 5d XAS spectra of Pu ions with different valences can be only found in the energy position of the pre-threshold structure relative to the main edge. In Figure 5-3, the calculated 5*d* absorption spectrum of Pu(IV) is compared with the experimental one /38/ for PUO_2. Relatively good agreement between the two spectra suggests that the atomic multiplet approach is still good approximation for the description of data of Pu compounds.

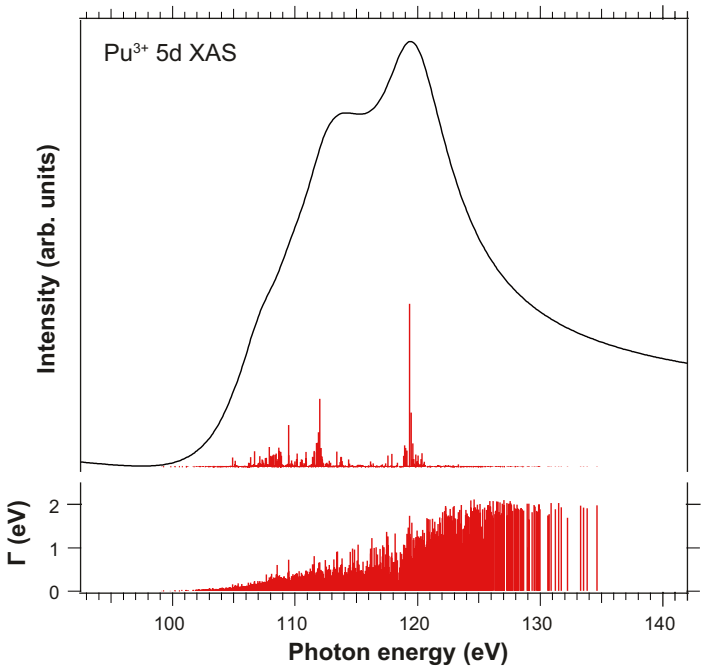

Figure 5-2. *Calculated 5d x-ray absorption of Pu(III) along with decay half-width (Γ) values.*

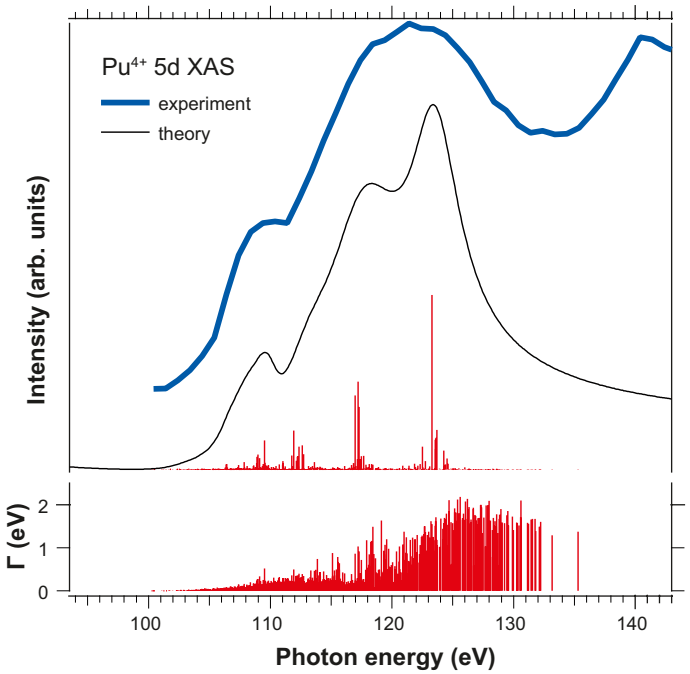

Figure 5-3. *Calculated Pu(IV) 5d x-ray absorption and experimental total-electron-yield spectrum38 of* PuO_2.

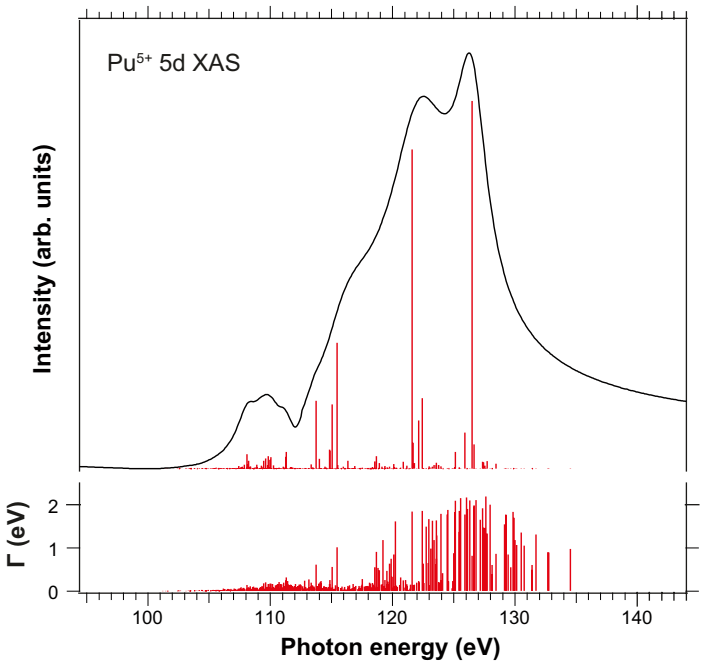

Figure 5-4. *Calculated 5d x-ray absorption of Pu(V) along with decay half-width (Γ) values.*

Figures 5-5 to 5-7 show theoretical x-ray scattering spectra of Pu(III), Pu(IV), and Pu(V) at various excitation energies across the 5*d* edge. The spectra were calculated in the same manner as for U(IV) and Np(IV) and using equation (2). The reduction of the Slater integrals was the same as in the calculations of the Pu 5*d* absorption spectra. The same scattering spectra are plotted on the energy loss scale in Figures 5-8 to 5-10. The RIXS profiles reveal significant dependence on the energy of the incident photons. Although, a substantial contribution to the RIXS profiles from ligand 2*p* →Pu 5*f* charge-transfer excitations in Pu compounds (neglected

in the calculations) can be expected for excitation energies set to the main Pu 5*d* edge, the *f-f* transitions should dominate RIXS spectra at the excitation energies tuned to the pre-threshold structures in 5*d* absorption spectra. Therefore, the RIXS spectra recorded at that photon energy range would be the best choice for a characterization of the oxidation state of Pu and for a comparison between different samples.

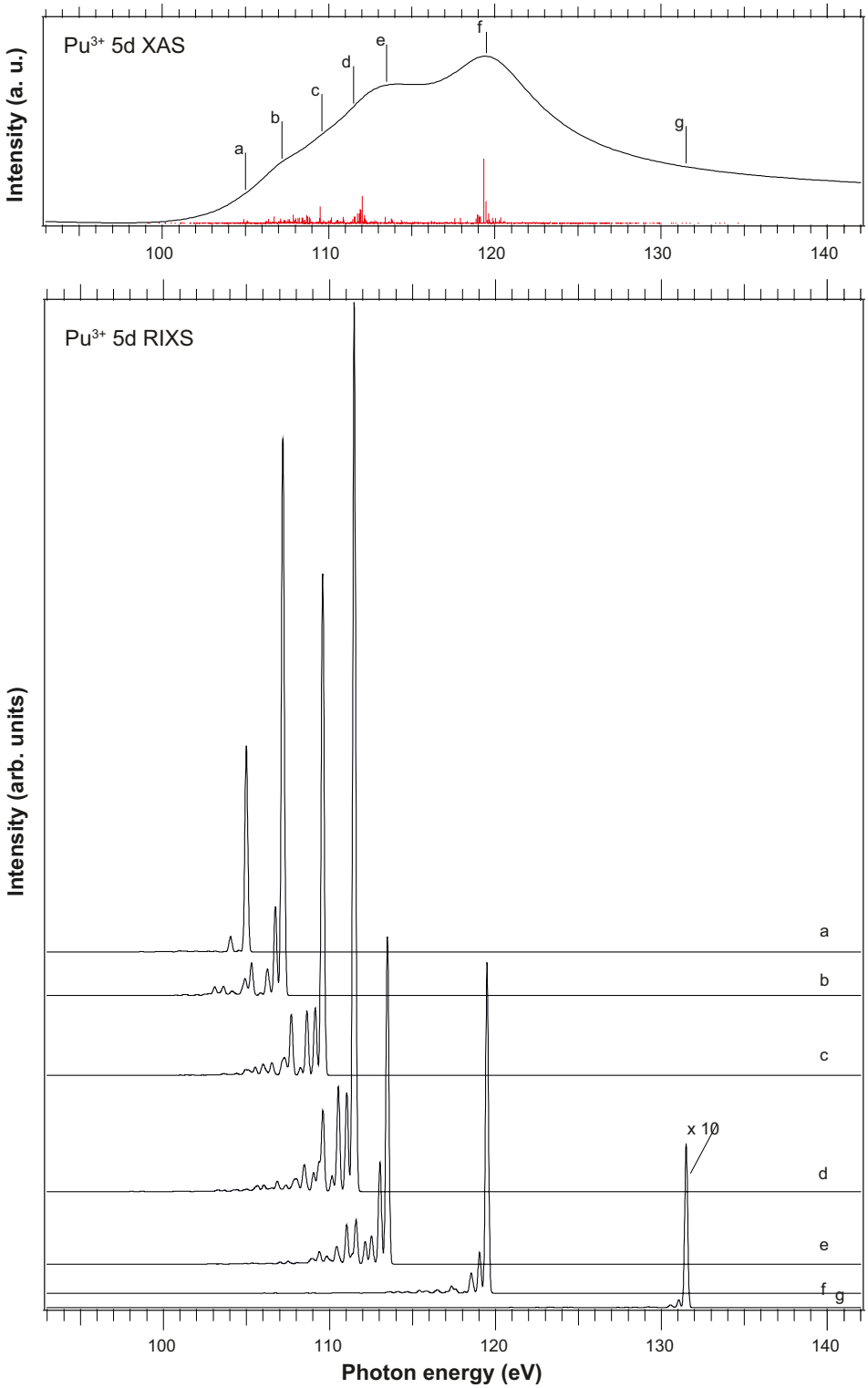

Figure 5-5. *Calculated resonant soft x-ray scattering spectra of Pu(III) at various excitation energies across the 5d edge indicated by letters on the corresponding absorption spectrum (top panel).*

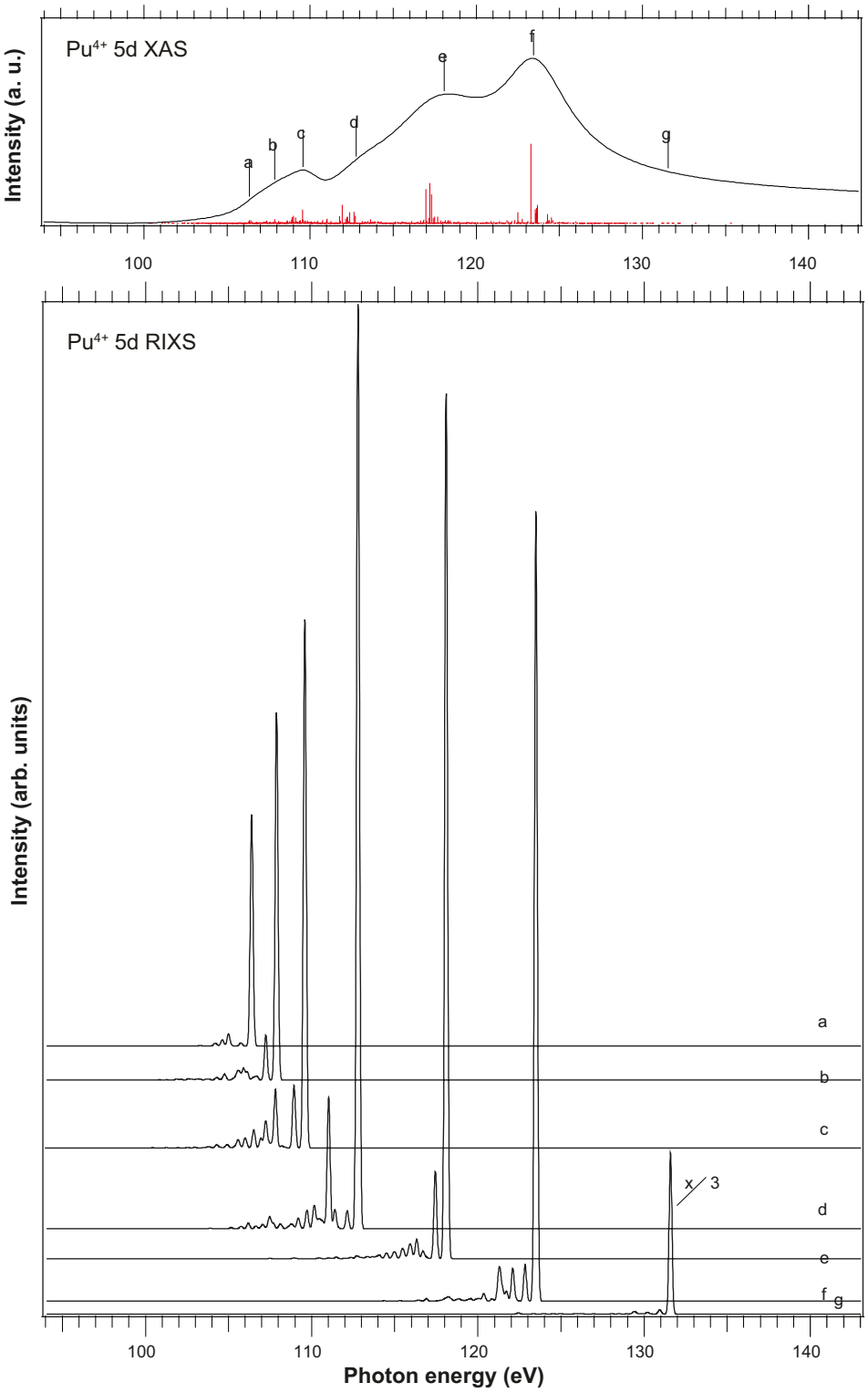

Figure 5-6. *Calculated resonant soft x-ray scattering spectra of Pu(IV) at various excitation energies across the 5d edge indicated by letters on the corresponding absorption spectrum (top panel).*

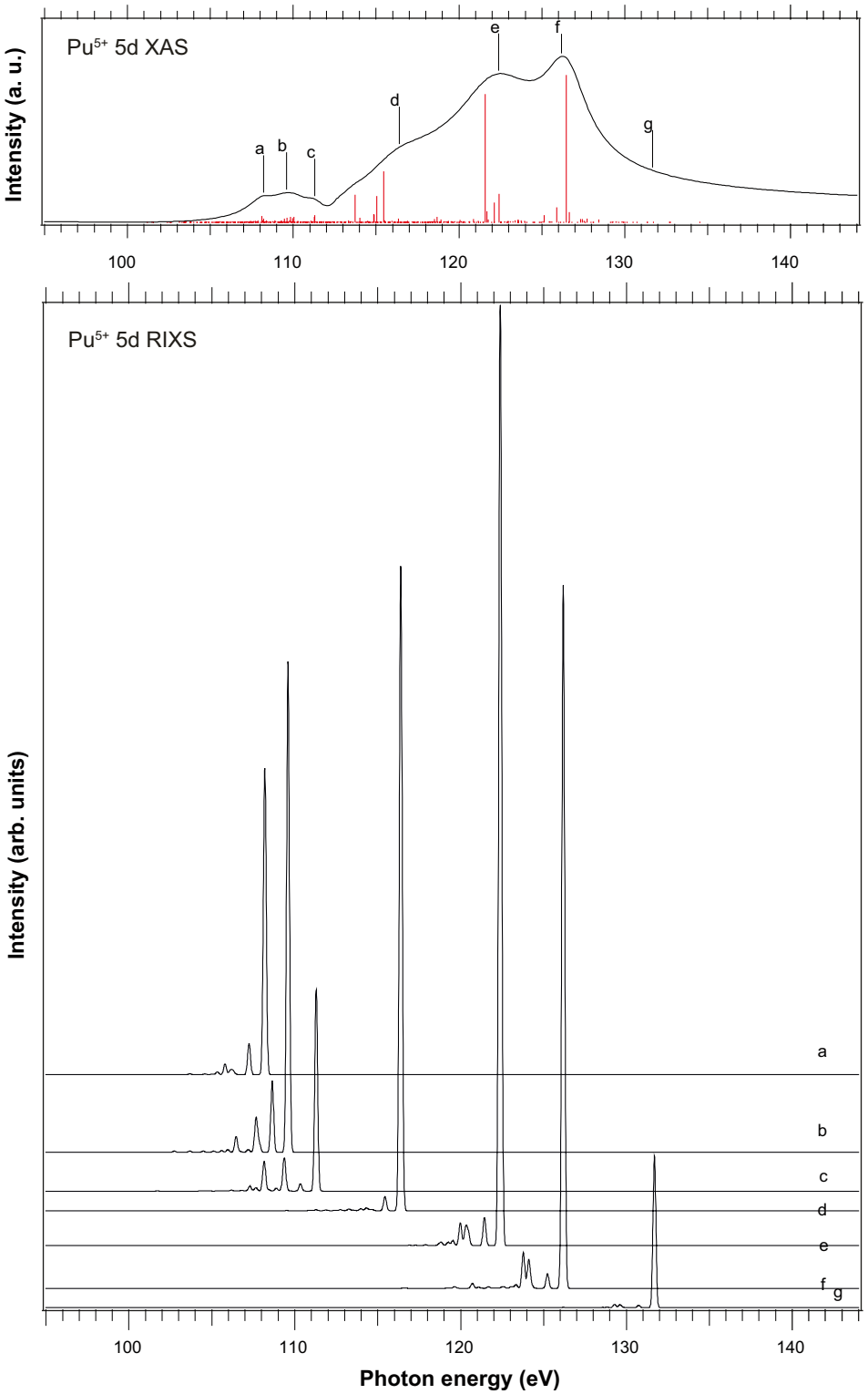

Figure 5-7. *Calculated resonant soft x-ray scattering spectra of Pu(V) at various excitation energies across the 5d edge indicated by letters on the corresponding absorption spectrum (top panel).*

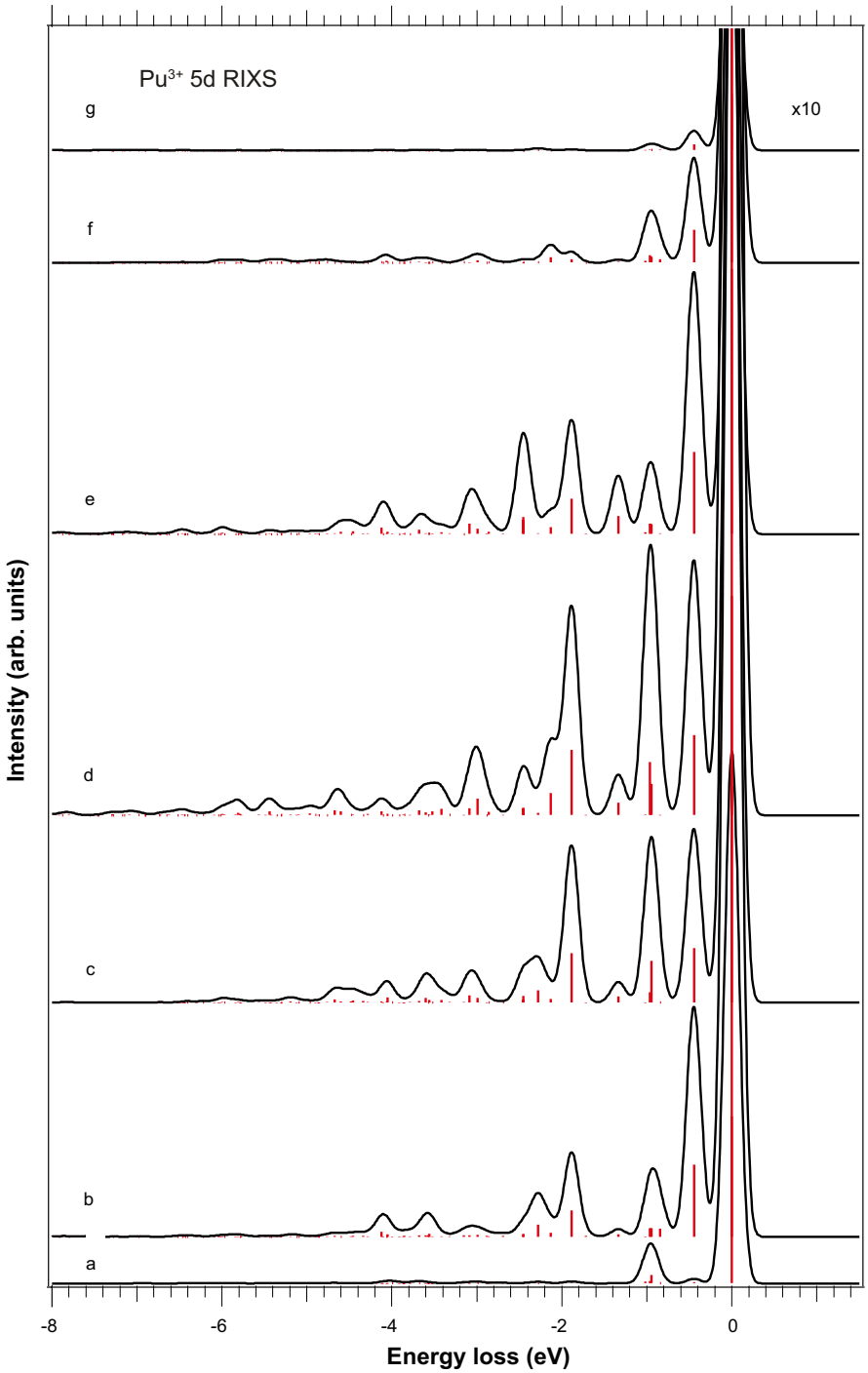

Figure 5-8. *The same spectra as in Figure 16 displayed on the energy loss scale.*

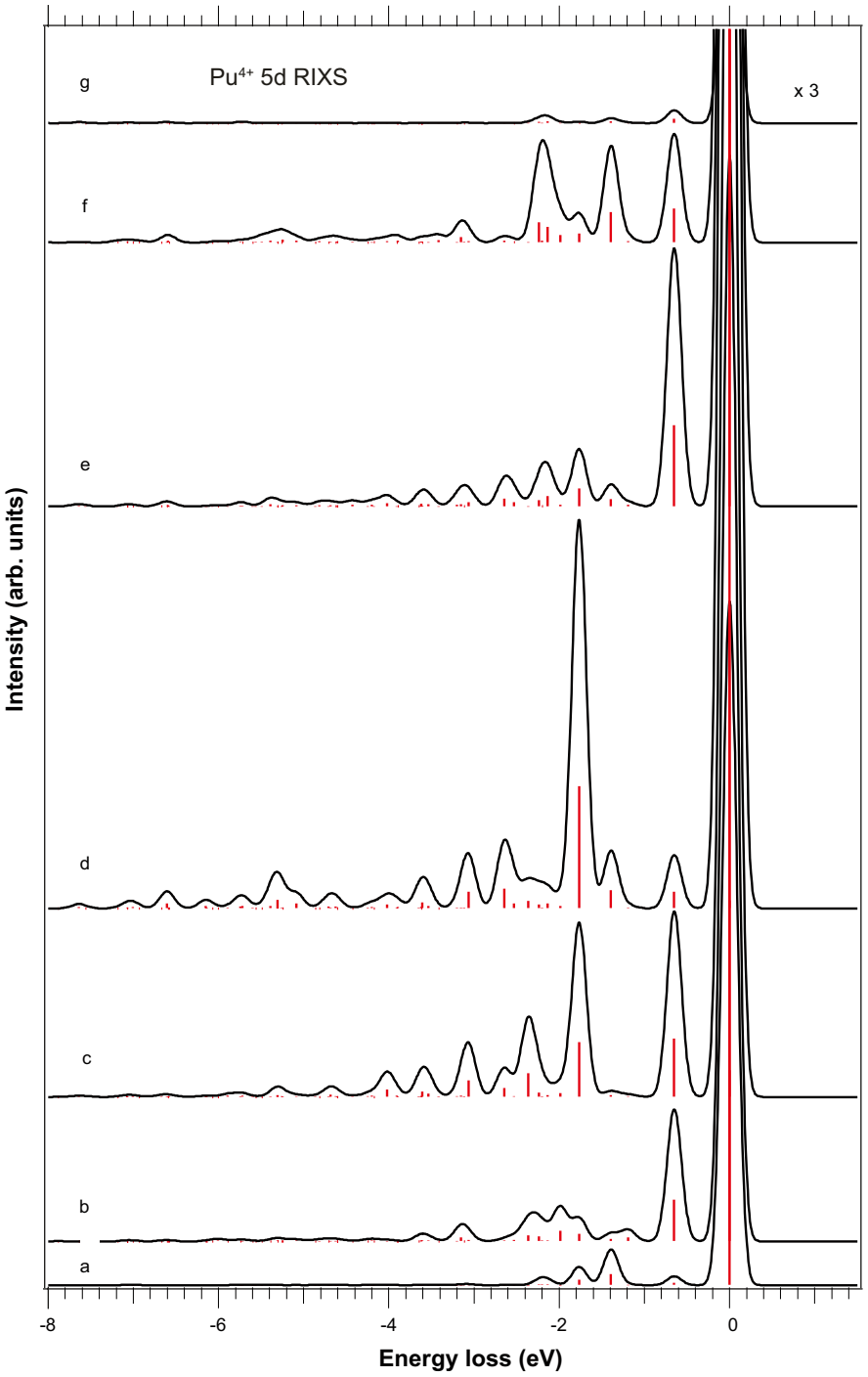

Figure 5-9. *The same spectra as in Figure 17 displayed on the energy loss scale.*

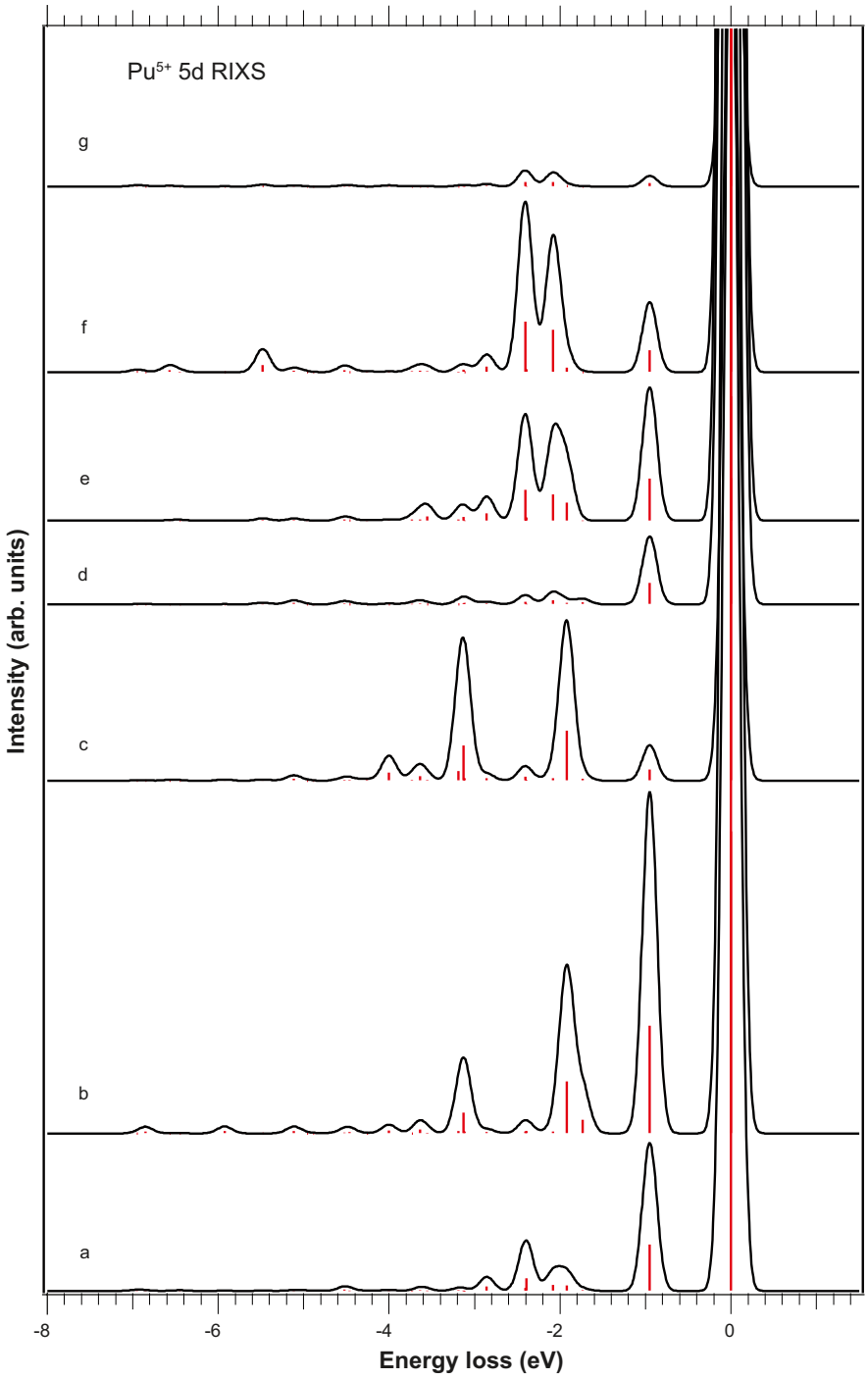

Figure 5-10. *The same spectra as in Figure 18 displayed on the energy loss scale.*

The results of calculations are in overall agreement with optical absorption data of Pu in various crystal matrices (e.g. /39–44/). The analysis of the optical data showed that crystal field splittings are similar to those in lanthanides, thus justifying the use of atomic multiplet theory as a good approximation for the description of high-energy spectroscopic data.

Figure 5-11 shows a comparison between calculated RIXS spectra of Pu(III), Pu(IV), and Pu(V) for an excitation energy of 109.6 eV, where the contribution of *f-f* transitions is expected to dominate the RIXS profiles. The three spectra reveal differences which are significant enough to distinguish between different oxidation states so that the technique can be employed, as in case of U and Np, to characterize the chemical state of Pu in various systems. In particular, a shift in the energy loss of major RIXS peaks can be used as a corresponding fingerprint.

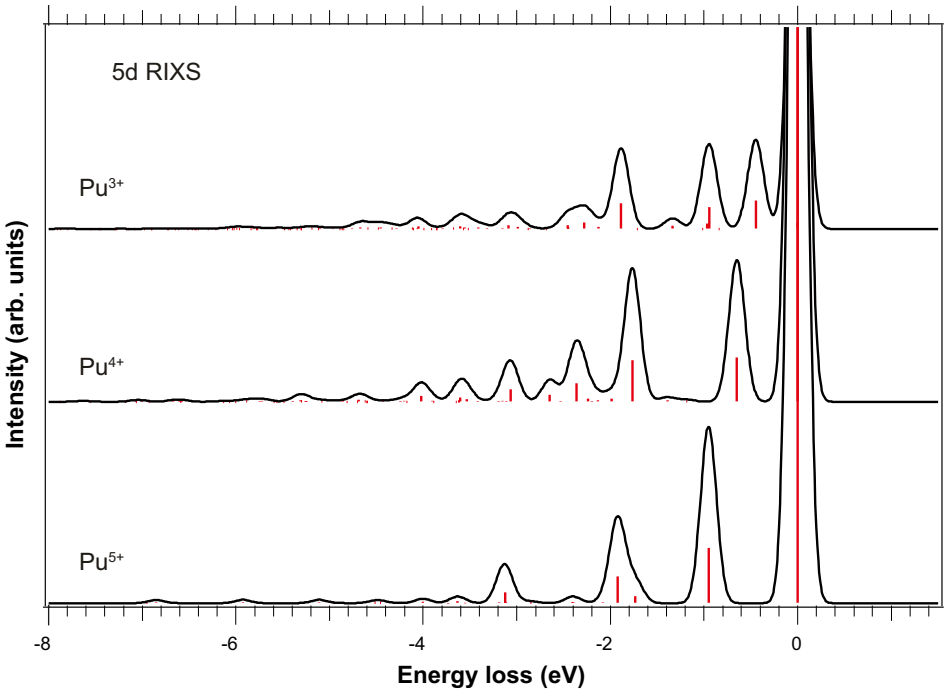

Figure 5-11. *Calculated resonant soft x-ray scattering spectra of Pu(III), Pu(IV), and Pu(V) at the excitation energy of 109.6 eV.*

5.2 Experimental setup and safety issues

The experiments were performed at undulator beamline 7.0 /45/ of the Advanced Light Source (ALS), Lawrence Berkeley National laboratory, employing a spherical grating monochromator and at undulator beamline I511-3 /46/ of Swedish synchrotron facility MAXLAB equipped with plane-grating monochromator SX-700. Resonant ultra-soft x-ray scattering spectra from the samples were recorded using a grazing-incidence grating spectrometer /47/ with a two-dimensional detector. Typical experimental set-up for RIXS measurements (as used at ALS) is shown as an optical layout in Figure 5-12 and in the photograph in Figure 5-13. The incidence angle of the photon beam was approximately 15° from the sample surface and the spectrometer was placed in the horizontal plane at an angle of 90° with respect to the incidence beam. The bandwidth of the excitation was about 65 meV. The total energy resolution of the RIXS data was estimated from the full width at half maximum of the elastic peak to be 160 meV.

Due to safety regulations at various synchrotron radiation facilities and difficulties to use samples as sealed, closed sources of radioactivity for soft x-ray spectroscopic measurements, we are forced to greatly minimize quantities of substances in question, in order to reduce the radiological risk to an acceptable level.

One of the measures for preventing radiological contamination of the experimental chamber is the use of specially designed sample holder (see Figure 5-14). It is essentially a cylindrical can with slots for incoming and outgoing radiation. The samples are attached to the slab inside the can just behind the slots. Due to this design, the sample holder served as a catch tray for material that might come loose during handling and the measurements, thus ensuring that no residuals will be left in the experimental chamber after the experiment.

Although, the sensitivity and selectivity of the RIXS technique is quite high, strict safety limitations on amounts of sample activity/quantity lower the contrast of measurements in some cases as one can see below. Considering that RIXS spectroscopy is a photon-hungry technique (due to low fluo-rescence yield as compared to electron yield per electronic excitation-deexcitation) and generally requires long acquisition times per spectrum, these limitations increase acquisition times even more.

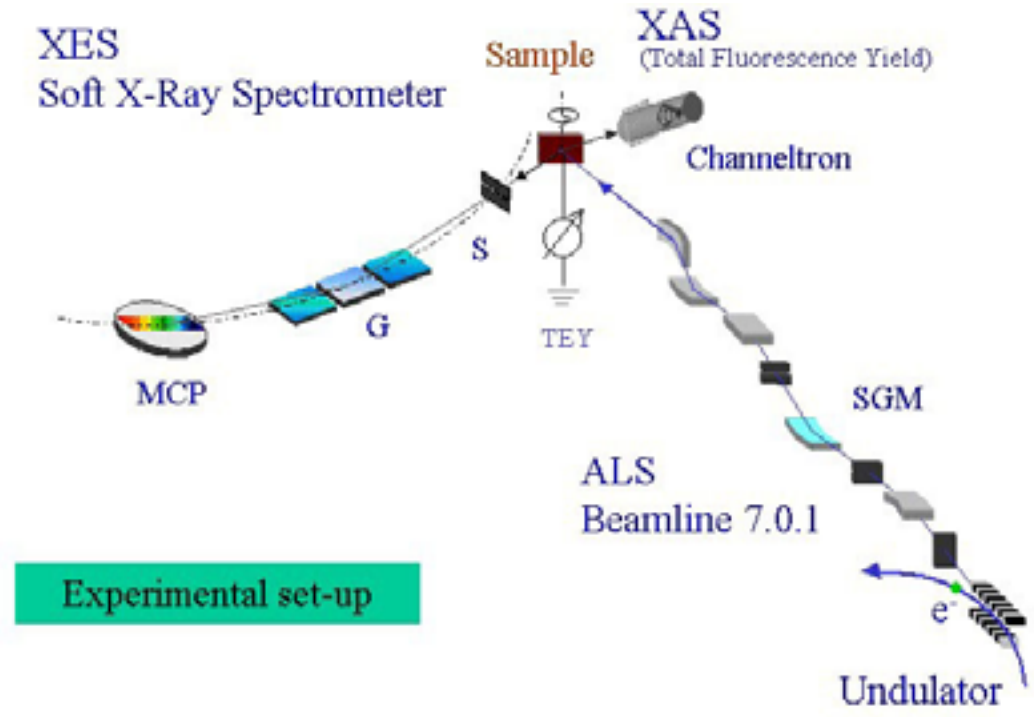

Figure 5-12. *Typical experimental setup for resonant inelastic soft x-ray scattering measurements as optical layout.*

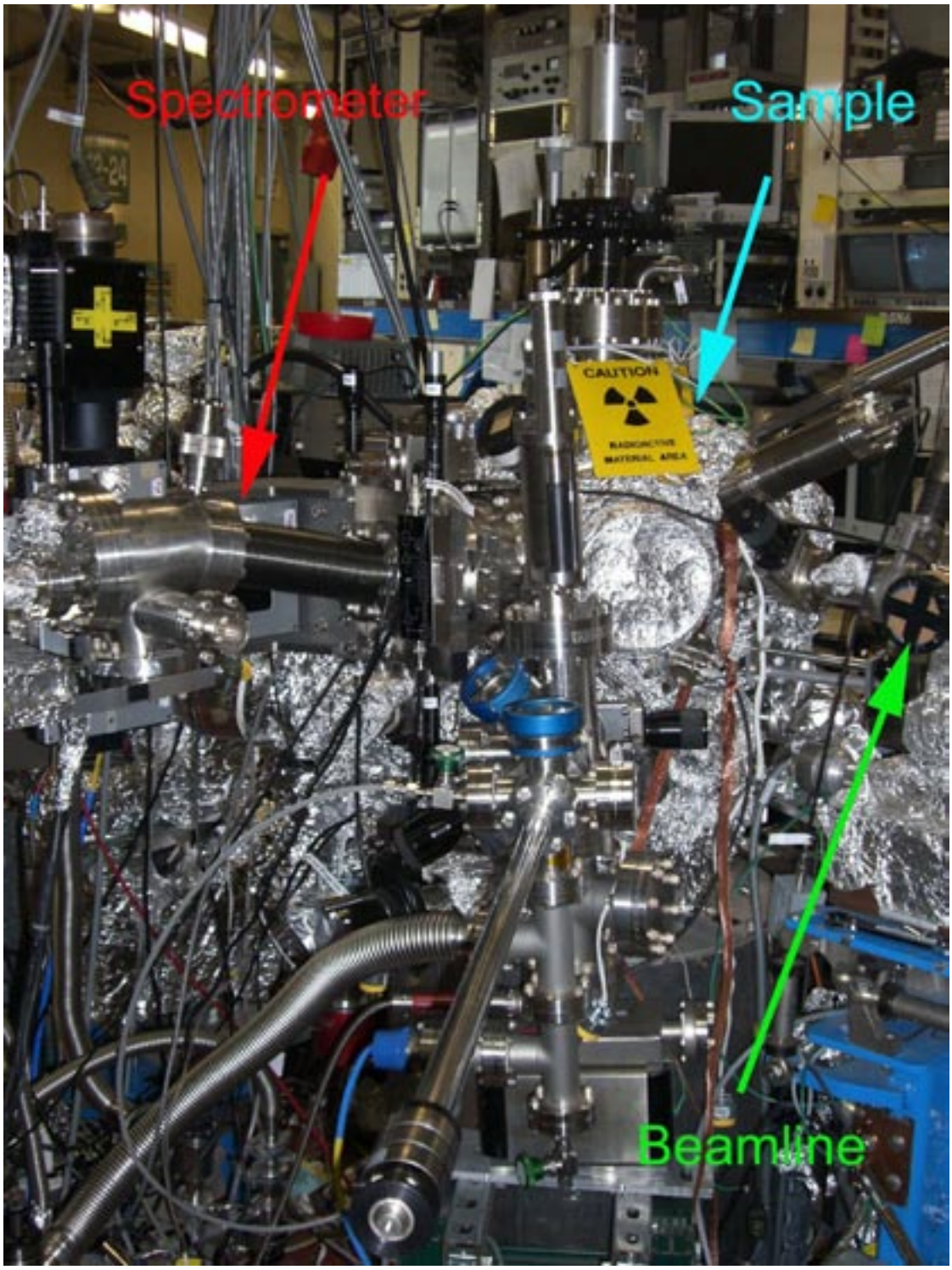

Figure 5-13. *Photograph of experimental setup for resonant inelastic soft x-ray scattering measurements.*

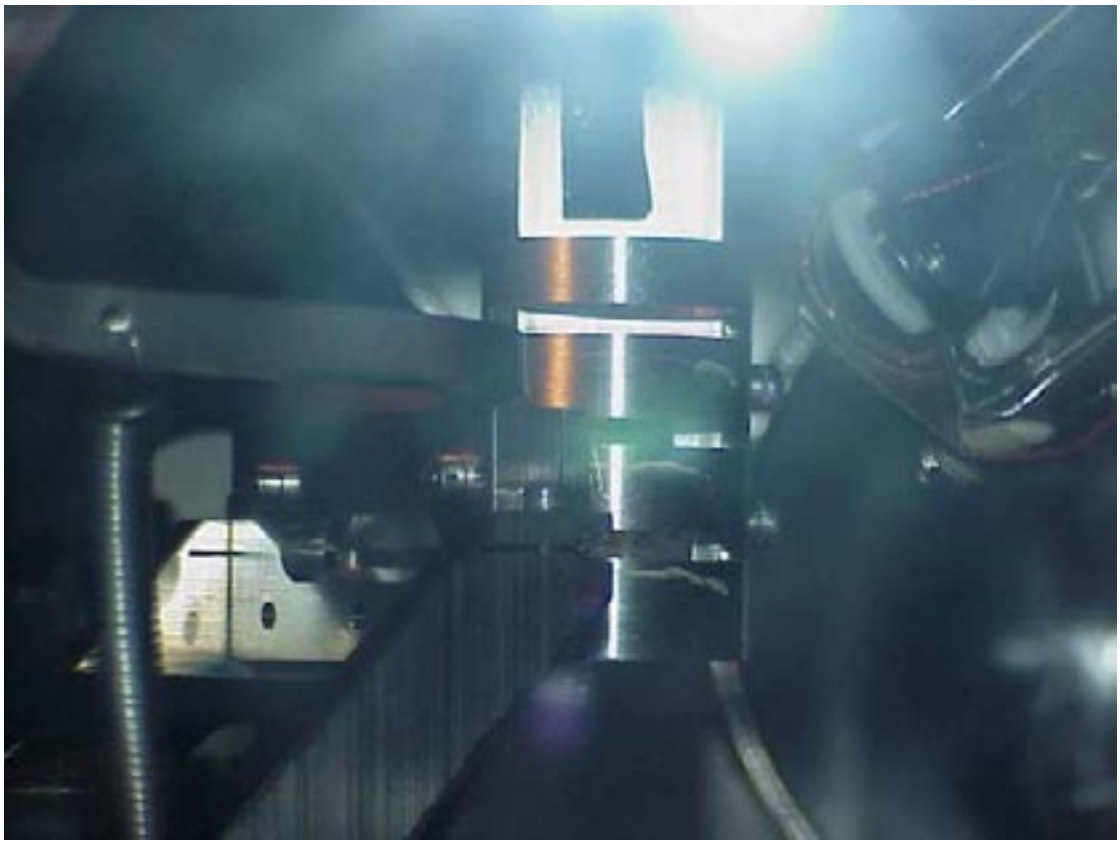

Figure 5-14. *Special sample holder (middle), designed for radioactive materials, shown inside the experimental chamber in between the spectrometer slit assembly (left) and channeltron (right).*

5.3 Sample preparation

Besides model calculations, it is helpful to have experimental data from reference samples where the oxidation state of actinide element is believed to be well defined.

The plutonium-242 dioxide sample used as a reference in present measurements was fabricated by standard techniques used to prepare radionuclide counting plates. The counting plate was prepared from an aqueous solution of about 0.8 mM plutonium-242 in approximately 0.1 M HCl that was localized onto the surface of high purity platinum substrate (25.4 mm diameter, 0.05 mm thickness) by successive, partial micro-pipette aliquots into an area of about 2 mm^2. The isotopic composition of the plutonium solution was about 99.9% plutonium-242 and 0.1% in the suite of Pu isotopes (238–241) by mass.

The aqueous solution was allowed to dry and the resulting solid residue was distributed in a ring-shaped manner. This structure was inductively heated to 700°C under atmosphere to oxidize the material and to fix the material onto the substrate to preclude loss in the UHV spectrometer chamber during the measurements. The final amount of Pu-242 on the counting plate was found to be about 1.2 μg.

The portion of the platinum counting plate containing the plutonium was cut into a to 4 mm x 4p mm square and mounted with conductive tape on a rectangular sample holder. For the Pu-on-Fe sample preparation, 10 ml of the Fe-equilibrated synthetic ground water and 0.7 ml of the Pu stock solution was mixed in a 20 ml glass vial containing a 2.5 x 4 mm iron strip. N_2 (g) was bubbled through the solution for a couple of minutes and the vial was closed with a screw cap. The vial was then put in a sealable plastic bag flushed with N_2, which was subsequently put inside a glass jar flushed with N_2. The lid of the glass jar was fitted with a rubber packing effectively sealing the lid. After 14 days the sample was opened and the pH, E_H, and the

Pu-concentration of the liquid mixture were measured (pH 9.7, E_H 335 mV, C_{Pu} 1.7E–7 M). There was some loose material (corrosion products and some staining of the Fe strip, especially on one side. This side had less Pu on it as measured by alpha spectrometry (197 Bq) as compared to the less stained side which had a Pu activity of 1341 Bq. This amounts to about half of the activity used in the experiment and the less stained side was that used for the RIXS measurement.

The plutonium stock solution was prepared by dissolving $^{242}PuO_2$ in a mixture of fairly concentrated $HClO_4$, HNO_3 and HF. From the resulting solution plutonium hydroxide was precipitated and separated using centrifugation. The precipitate was wash twice with deionized water and was then dissolved in 1.5 M $HClO_4$. Undissolved residues were again separated using centrifugation and discarded. Using a electrochemical cell with an Ag/AgCl reference electrode and Pt working and auxiliary electrodes connected to a potentiostat (EG&G Instr. Princeton Applied Research Model 283) the plutonium in solution was oxidized to Pu(VI). After the oxidation, the pH of the solution was adjusted to slightly basic using solutions of NaOH at different concentrations. During this adjustment the solution was diluted about one order of magnitude. The solution was left to stand for a couple of days before the first use and a white fluffy precipitate was observed which settled nicely to the bottom of the vial. The pH and plutonium concentrations where measured to 9.4 and 0.1 mM. This is far above the solubility of Pu(IV) at this pH indicating that the Pu is stable in the pentavalent or hexavalent state. The stock solution was centrifuged a final time just prior to the sample preparation and the precipitate was discarded.

A synthetic groundwater was prepared according to Vourinen and Snellman /48/ and with the approximate composition given in Table 5-1.

All centrifugation was made using a Fisher Scientific MicroV centrifuge at 10,000 rpm for 10 minutes. All water was initially Millipore MQ-grade.

The method described above was also used to prepare another sample of Pu sorbed on the Fe foil with lower Pu content/activity, as low as 2.3 nCi.

Table 5-1. Composition of ground water with pH 8.8

	(mg/L)	(mmol/L)
Na^+	52.5	2.3
Ca^{2+}	5.1	0.13
Mg^{2+}	0.7	0.03
K^+	3.9	0.10
SiO_2	1.7	0.03
SO_4^{2-}	9.6	0.10
Cl^-	48.8	1.4
HCO_3^-	65.0	1.1

5.4 Experimental results

Figure 5-15 displays x-ray absorption and resonant x-ray scattering spectra of so-called reference sample/counting plate recorded throughout the Pu 5d edge. The x-ray absorption spectrum is broad due to autoionization effects and in general agreement with the calculated spectrum for Pu(IV), although when comparing the latter with the calculated spectrum for Pu(V), a large broadening makes difference between the spectra marginal. RIXS spectra which were measured at an energy of the incident photon beam tuned to various parts of the Pu 5d absorption edge are plotted in Figure 5-15 on the energy loss scale. RIXS spectra reveal a number of structures showing dependence on varying energies of incident photons. In particular, structures at energy losses of –0.8, –1.1, –1.6 and –1.8 eV can be identified in some RIXS spectra. Important resonant behavior can be noted for the –1.6 eV and –1.8 eV structures which are marked by blue and green dashed vertical lines, respectively, in Figure 5-15. The former is significant in the RIXS spectrum recorded at the excitation energy of 109.5 eV and again becomes pronounced for energies of incident photons being in the range 113–115 eV, while the latter resonates at excitation energies tuned between 110 and 112.5 eV.

On going to the Pu-on-Fe system, first, the sample with lower activity (2.3 nCi) was studied. As a result, a comparison of spectra recorded at two different energies of incident photons with those of the reference sample is made in Figures 5-16 and 5-17. The excitation energies were chosen to represent two regions for which the resonances of RIXS structures at energy losses of –1.6 and –1.8 eV were respectively detected for the reference sample. Although, due to a low content of Pu and an intense contribution of reflectivity in the elastic peak, the signal-to-noise ratio for the useful RIXS signal is reduced, it is still possible to detect RIXS structures.

While the spectra of the reference Pu dioxide and the sample of Pu sorbed on the Fe surface are similar to each other in terms of existing spectral structures and their energies in Figure 5-16, they are somewhat different from each other in this respect in Figure 5-17. An interesting finding from the measurements is that the resonance of the –1.8 eV structure is missing in the RIXS spectra of the Pu-on-Fe sample. An inspection of RIXS profiles in Figure 5-17 shows that only the neighboring –1.6 eV structure is present for the Pu-on-Fe sample under conditions favorable for the –1.8 eV resonance, as found for the spectrum of the reference sample.

Similar results were obtained for the sample with larger quantity of Pu sorbed on the Fe foil which are displayed in Figures 5-18 and 5-19. Note that RIXS spectra of the Pu-on-Fe sample in these figures, which were measured at specific excitation energies leading to above-discussed resonant effects for the reference Pu dioxide, resemble each other in terms of observed RIXS structures and their energies quite closely in contrast to the data for the reference sample. Both spectra of sorbed Pu reveal main RIXS peaks at energy losses of about –0.7 eV and – 1.6 eV.

The energy scale of the RIXS structures observed in Figures 5-15 to 5-19 allows to assign them to spectral transitions which are a result of *f-f* excitations within the Pu 5*f* shell. Therefore, the results of the model atomic-multiplet calculations for Pu ions in various oxidation states can be used to aid the interpretation of the experimental data.

When comparing calculated scattering spectra of Pu(III), Pu(IV), and Pu(V) ions in Figure 5-11 (calculated for an excitation energy of 109.6 eV) with the experimental spectrum of the reference sample from Figure 5-15, which was recorded at the energy of incident photons of 109.5 eV, we find that the calculated RIXS profile for Pu(IV) is in better agreement with the experimental one. Calculated main RIXS peaks at –0.65 eV and –1.75 eV can be related to structures at –0.8 eV and –1.6 eV in the experimental spectrum, respectively. At the same time, the results of calculations for Pu(III) contain too many peaks while the calculated two main RIXS peaks in spectrum of Pu(V) are shifted by 0.2 eV to higher energy losses as compared to those calculated for Pu(IV).

When analyzing other experimental RIXS data measured on the reference sample, for example, the shape of the spectrum for the excitation energy of 115.0 eV can be reproduced as a superposition of two Pu(IV) RIXS spectra calculated for excitation energies of 112.8 eV and 118.1 eV, respectively (since the calculations were performed before the RIXS experiments were carried out, there is no calculated spectrum available for exactly the same excitation energy of 115.0 eV). The RIXS part of the experimental 115.0 eV spectrum is dominated by two structures at energy losses of –0.8 eV and –1.6 eV as in case of the discussed above 109.6 eV spectrum. Therefore, these structures can be considered intrinsic to Pu(IV) as a result of *f-f* excitations.

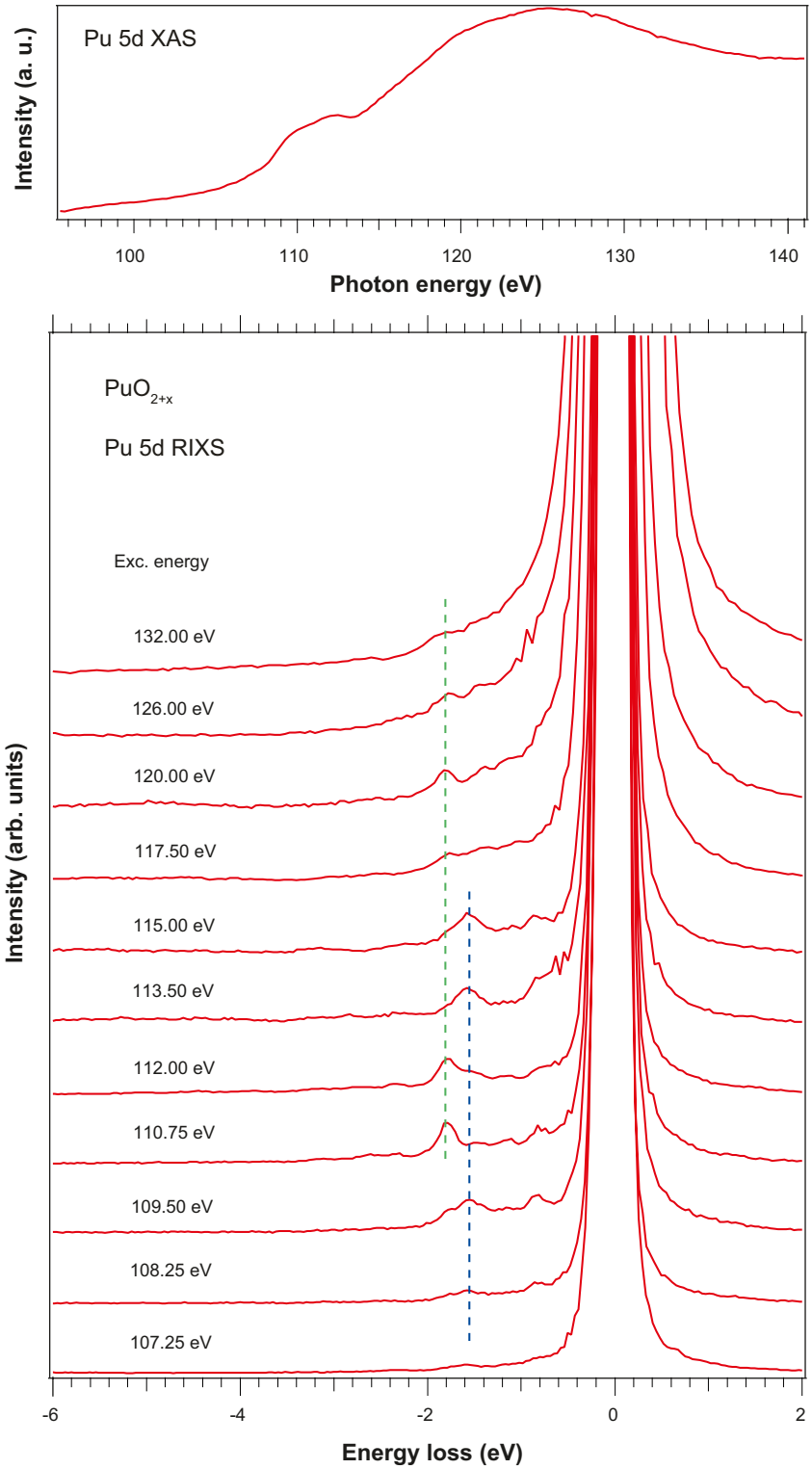

Figure 5-15. *Resonant x-ray scattering spectra of Pu dioxide recorded at different excitation energies close to the Pu 5d threshold. The Pu 5d absorption edge recorded in the total electron yield mode is shown in the top panel.*

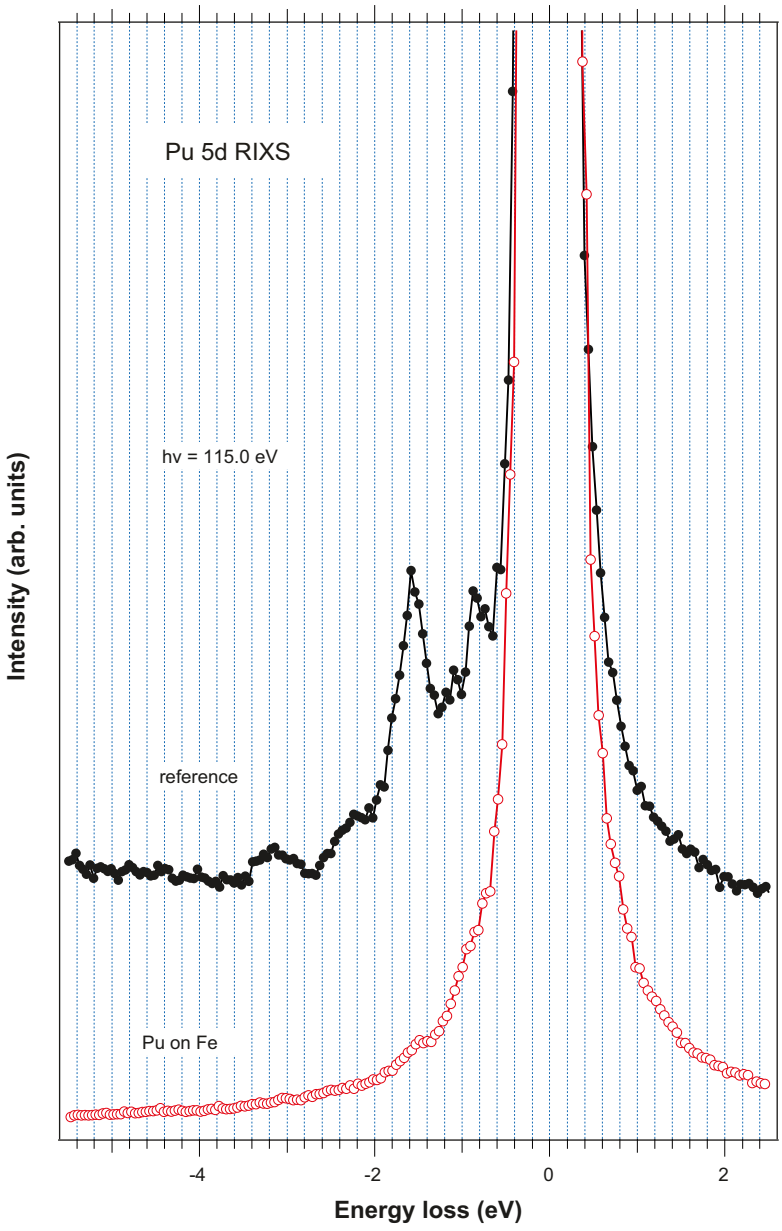

Figure 5-16. *Comparison of resonant inelastic soft x-ray scattering spectra of Pu sorbed on the Fe strip (sample with low activity) and Pu dioxide at the energy of incident photons tuned to 115.0 eV.*

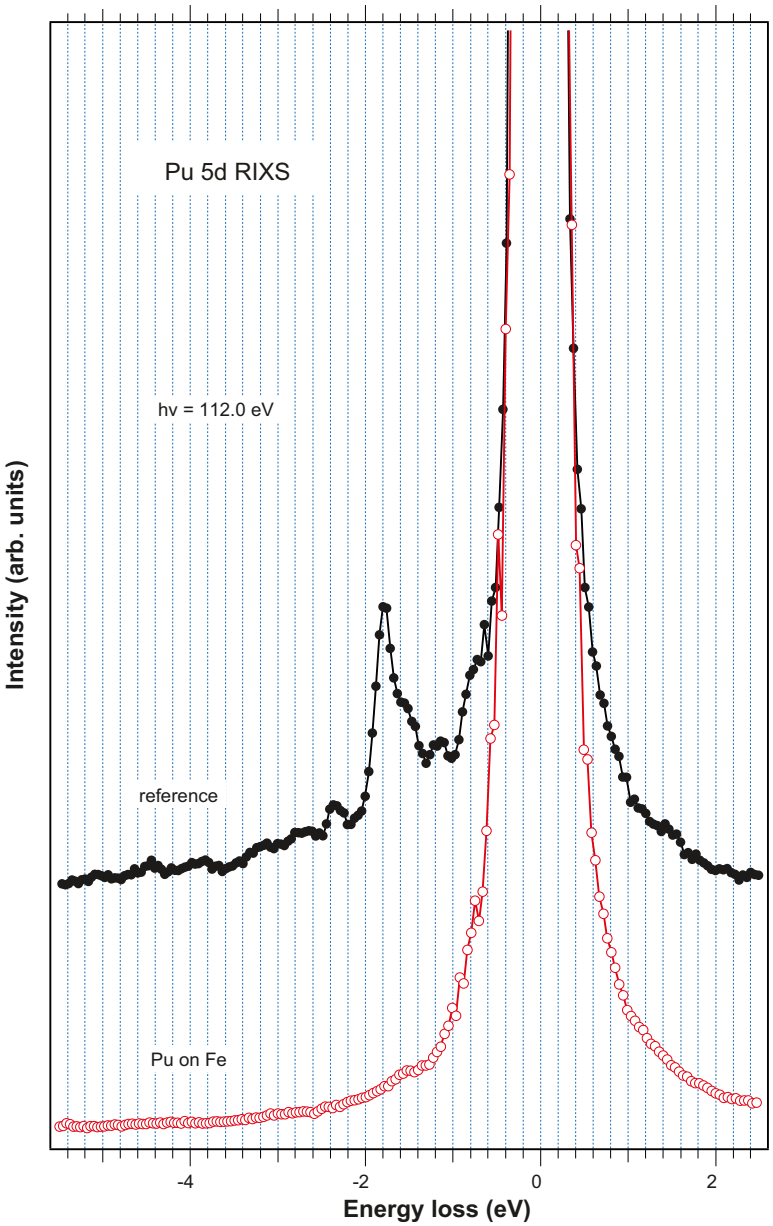

Figure 5-17. *Comparison of resonant inelastic soft x-ray scattering spectra of Pu sorbed on the Fe strip (sample with low activity) and Pu dioxide at the energy of incident photons tuned to 112.0 eV.*

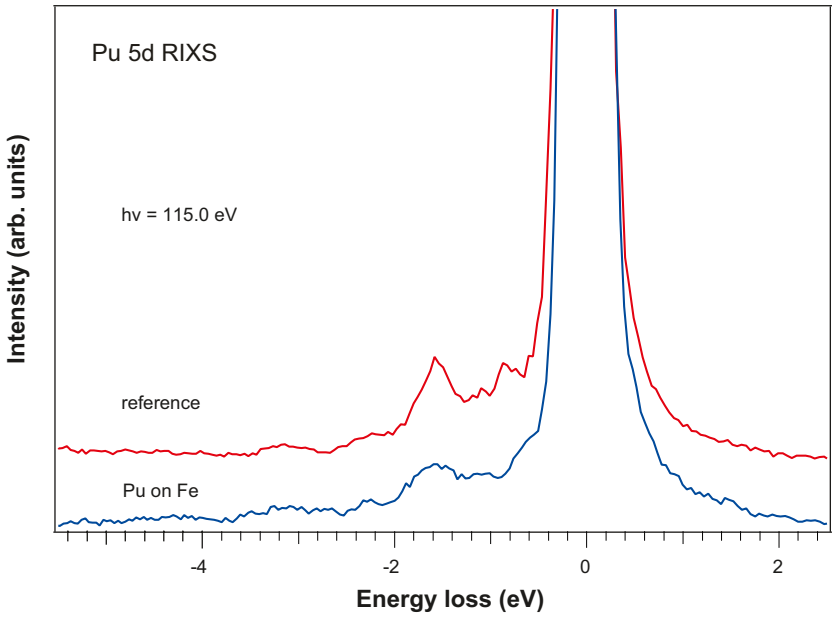

Figure 5-18. *Comparison of resonant inelastic soft x-ray scattering spectra of Pu sorbed on the Fe strip (sample with high activity) and Pu dioxide at the energy of incident photons tuned to 115.0 eV.*

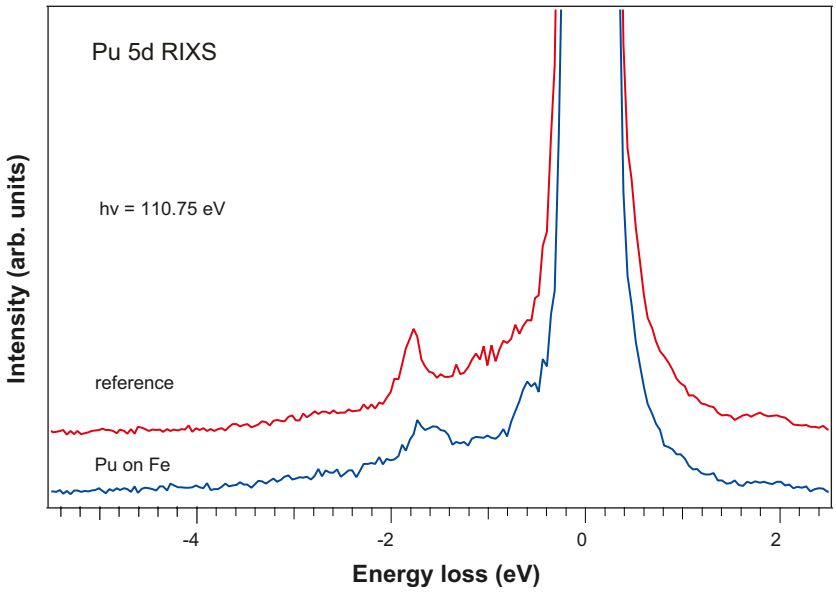

Figure 5-19. *Comparison of resonant inelastic soft x-ray scattering spectra of Pu sorbed on the Fe strip (sample with high activity) and Pu dioxide at the energy of incident photons tuned to 110.75 eV.*

Turning to Pu-on-Fe samples, the measured RIXS spectra reveal the presence of these structures and RIXS profiles are in agreement with those calculated for the Pu(IV) ion. This strongly suggests that plutonium from the Pu(VI) solution sorbed on Fe surfaces is getting reduced and Pu species sorbed on the Fe foils are mainly in the form of Pu(IV).

What is the origin of the resonating structure which is clearly observed in the RIXS spectra of the reference sample of the Pu dioxide and is not detected for the Pu-on-Fe samples? We attribute it to the presence of some Pu(V) fraction in the reference sample. According to calculations (see Figure 5-11), the main RIXS peaks of Pu(V) are shifted to higher energy losses by 0.2 eV which matches exactly the energy difference between structures at –1.6 eV, which is believed to belong to Pu(IV), and at –1.8 eV in the measured RIXS spectra. Due to selectivity

properties of the RIXS technique, differences in the absorption and resonant scattering cross-sections for Pu(IV) and Pu(V), it is quite reasonable to expect that the relative intensity of the Pu(V) contribution can be enhanced versus that of Pu(IV) in the RIXS spectra for specific excitation energies. The presence of the Pu(V) fraction in the reference sample may be due to its preparation procedure or/and specific conditions under which further oxidation of PuO_2 may take place as it has been discussed in scientific literature. /49/

The presence of some fraction of Pu in higher oxidation state than Pu(IV) in the reference sample is also supported by Pu 4*d* x-ray absorption measurements (see Figure 5-20). The Pu 4*d* x-ray absorption spectrum of the reference is shifted to higher-energies by approximately 0.3 eV and narrower as compared to that of the high-activity Pu-on-Fe sample. This behavior indicates higher average charge of Pu atoms in the reference sample. On the other hand, analysis of RIXS spectra does not support the presence of Pu(III) in the Pu-on-Fe samples.

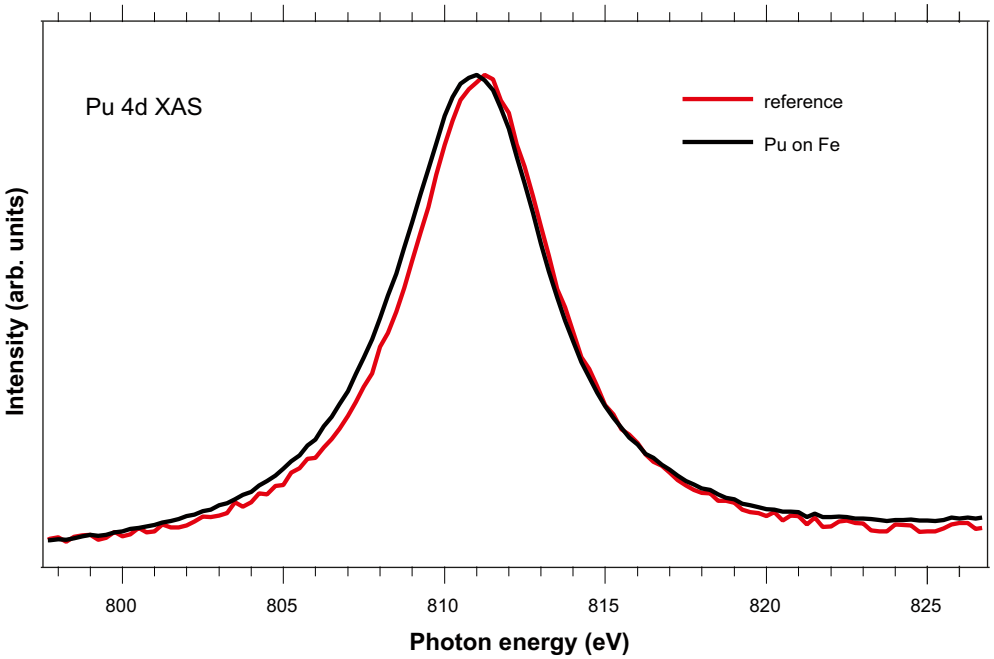

Figure 5-20. *Total electron yield spectra of Pu dioxide reference and Pu sorbed on Fe foil across the U 4d absorption edge.*

6 Conclusion

Based on analysis of spectral shapes, their dependence on the energy of incident photons and comparison with model calculations and experimental data from the reference sample we can conclude that plutonium from the Pu(VI) solution sorbed on Fe surfaces is likely to be reduced and Pu species sorbed on the Fe foils are mainly in the form of Pu (IV). Current results correlate with what was observed for for Np (V) and U (VI) in our previous studies. Furthermore, combined analysis of present data with model atomic multiplet calculations of RIXS and XAS spectra suggests that significant presence of Pu(III) on the Fe foils is unlikely.

7 References

/1/ **P W Anderson.** Phys. Rev. B, 124 (1961) 41.

/2/ **J Zaanen, G A Sawatzky, J W Allen.** Phys. Rev. Lett. 55 (1985) 418.

/3/ **O Gunnarsson, O Jepsen.** Phys. Rev. B, 38 (1988) 3568; **O Gunnarsson, O K Andersen, O Jepsen, J Zaanen,** ***ibid.*** 39 (1989) 1708; **O Gunnarsson, K Schönhammer,** ***ibid.*** 40 (1989) 4160; **O Gunnarsson, N E Christensen,** ***ibid.*** 42 (1990) 2363.

/4/ **P Kuiper, J-H Guo, C Såthe, L-C Duda, J Nordgren, J J M Pothuizen, F M F de Groot, G A Sawatzky.** Phys. Rev. Lett. 80 (1998) 5204.

/5/ **Y Ma, N Wassdahl, P Skytt, J Guo, J Nordgren, P D Johnson, J-E Rubensson, T Boske, W Eberhardt, S D Kevan.** Phys. Rev. Lett. 69 (1992) 2598.

/6/ **S M Butorin, D C Mancini, J-H Guo, N Wassdahl, J Nordgren, M Nakazawa, S Tanaka, T Uozumi, A Kotani, Y Ma, K E Myano, B A Karlin, D K Shuh.** Phys. Rev. Lett. 77 (1996) 574.

/7/ **B T Thole, G vand der Laan, M Fabrizio.** Phys. Rev. B, 50 (1994) 11466.

/8/ **S Tanaka, A Kotani.** J. Phys. Soc. Jpn. 62 (1993) 464.

/9/ **S M Butorin, J-H Guo, M Magnuson, P Kuiper, J Nordgren.** Phys. Rev. B. 54 (1996) 4405.

/10/ **S M Butorin, D-C Mancini, J-H Guo, N Wassdahl, J Nordgren.** Journal of Alloys and Compounds, 225 (1995) 230.

/11/ **A Kotani.** J Electr. Spectrosc. 110–111 (2000) 197.

/12/ **S M Butorin, J-H Guo, M Magnuson, J Nordgren.** Phys. Rev. B, 55 (1997) 4242.

/13/ **S M Butorin, L-C Duda, J-H Guo, N Wassdahl, J Nordgren, M Nakazawa, A Kotani.** J. Phys.: Condens. Matter, 9 (1997) 8155.

/14/ **S M Butorin, M Magnuson, K Ivanov, D K Shuh, T Takahashi, S Kunii, J-H Guo, J Nordgren.** J. Electr. Spectrosc. 101–103 (1999) 783.

/15/ **R D Cowan.** *The Theory of Atomic Structure and Spectra* (University of California Press, Berkeley, 1981).

/16/ **J Sugar.** Phys. Rev. B, 5 (1972) 1785.

/17/ **A Kotani, H Ogasawara.** J. Electr. Spectrosc. & Rlt. Phenom. 60 (1992) 257.

/18/ **H Ogasawara, A Kotani.** J. Phys. Soc. Jpn.64 (1995) 1394.

/19/ **S M Butorin.** J. Electr. Spectrosc. 110-111 (2000) 233.

/20/ **J J Pireaux, J Riga, E Thibaut, C Tenret-Noël, R Caudino, J J Verbist.** Chem. Phys. 22 (1977) 113.

/21/ **Yu A Teterin, V M Kulakov, A S Baev, N B Nevzorov, I V Melnikov, V A Streltsov, L G Mashirov, D N Suglobov, A G Zelenkov.** Phys. Chem. Minerals, 7 (1981) 151.

/22/ **H Madhavaram, P Buchanan, H Idriss.** J. Vac. Sci. Technol. A 15 (1997) 1685.

/23/ **J J Verbist, J Riga, C Tenret-Noël, J J Pireaux, G Dúrsel, R Caudino, E G Derouane,** in *Plutonium and other actinides*, **eds. H Blank, R Lindner** (North-Holland, Amsterdam, 1976), p.409.

/24/ **G C Allen, A J Griffiths, C W Suckling.** Chem. Phys. Lett. 53 (1978) 309.

/25/ **V A Gubanov, A Rosén, D E Ellis.** Solid State Commun. 22 (1977) 219.

/26/ **V Heera, G Seifert, P Ziesche.** Phys. Stat. Sol. (b), 118 (1983) K107.

/27/ **D E Ellis, G L Goodman.** Int. J. Quant. Chem. 25 (1984) 185.

/28/ **G L Goodman.** Journal of Alloys and Compounds, 181 (1992) 33.

/29/ **O Gunnarsson, D D Sarma, F U Hillebrecht, K Schönhammer.** J. Appl. Phys. 63 (1988) 3676; **O Gunnarsson, T C Li.** Phys. Rev. B, 36 (1987) 9488.

/30/ **A Kotani, H Ogasawara.** Physica C, 186–188 (1993) 16.

/31/ **K Pierloot, A Reinders, G L Goodman, D Devoghel, C Görller-Walrand, L G Vanquickenborne.** J. Chem. Phys. 94 (1991) 2928.

/32/ **P F Walsh, D E Ellis.** J. Chem. Phys. 65 (1976) 2387.

/33/ **J H Wood, M Boring, S B Woodruff.** J. Chem. Phys. 74 (1981) 5225 and references therein.

/34/ **L E Cox.** J. Electr. Spectrosc. 26 (1982) 167.

/35/ **J B Gruber, E R Menzel.** J. Chem. Phys. 50 (1969) 3772.

/36/ **C K Jørgensen.** J. Inorg. Nucl. Chem. 1 (1955) 301.

/37/ **H Ogasawara, A Kotani, B T Thole, K Ichikawa, O Aita, M Kamada.** Solid State Commun. 81 (1992) 645.

/38/ **D K Shuh et al.** unpublished results.

/39/ **A M Leontovich.** Opt. i Spektroskopiya, 2 (1957) 695.

/40/ **H Lämmerman, H P Stapleton.** J. Chem. Phys. 35 (1961) 1514; *ibid.* **H Lämmerman, J G Conway, *ibid.*** 38 (1963) 259.

/41/ **R McLaughlin, R White, N Edelstein, J G Conway.** J. Chem. Phys. 48 (1968) 967.

/42/ **N Edelstein, H F Mollet, W C Easley, R J Mehlhorn.** J. Chem. Phys. 51 (1969) 3281.

/43/ **L P Varga, M J Reisfeld, L B Asprey.** J. Chem. Phys. 53 (1970) 250.

/44/ **W T Carnall, P R Fields, R G Pappalardo.** J. Chem. Phys. 53 (1970) 2922.

/45/ **T Warwick, P Heimann, D Mossessian, W McKinney, H Padmore.** Rev. Sci. Instrum. 66 (1995) 2037.

/46/ **R Denecke, P Väterlein, M Bässler, N Wassdahl, S Butorin, A Nilsson, J-E Rubensson, J Nordgren, N Mårtensson, R Nyholm.** J. Electron Spectrosc. 101–103 (1999) 971.

/47/ **J Nordgren, G Bray, S Cramm, R Nyholm, J-E Rubensson, N Wassdahl.** Rev. Sci. Instrum. 60 (1989) 1690.

/48/ **U Vuorinen, M Snellman.** Finnish reference waters for solubility, sorption and diffusion studies. Helsinki, Finland: Posiva Oy, Posiva Working Report 98-61 (1998), 41 p.

/49/ **P A Korzhavyi, L Vitos, D A Andersson, B Johansson.** Nature Materials, 3 (2004) 225.

ISSN 1404-0344
CM Gruppen AB, Bromma, 2009